

**Orientation of fibres in suspensions flowing over  
a solid surface**

by

Allan Carlsson

January 2007  
Technical Reports from  
Royal Institute of Technology  
KTH Mechanics  
SE - 100 44 Stockholm, Sweden

Akademisk avhandling som med tillstånd av Kungliga Tekniska Högskolan i Stockholm framlägges till offentlig granskning för avläggande av teknologie licentiatexamen fredagen den 23 februari 2007 kl 9.00 i Sundbladssalen, Drottning Kristinas väg 61, STFI-Packforsk, Stockholm.

©Allan Carlsson 2007

Universitetsservice US-AB, Stockholm 2007

# Orientation of fibres in suspensions flowing over a solid surface

Allan Carlsson 2007

Linné Flow Centre

KTH Mechanics

SE - 100 44 Stockholm, Sweden

## Abstract

The orientation of fibres suspended in a viscous fluid, flowing over a solid surface, has been studied experimentally. A shear layer was generated, by letting the suspension flow down an inclined plate. Far upstream from the measuring section the suspension was accelerated to obtain an initial orientation of the fibres aligned with the flow direction. A CCD-camera was used to visualise the fibres. The velocity profile of the fibres coincided with the theoretical expression for fully developed flow of Newtonian liquid down an inclined wall.

The orientation of the fibres was analysed in planes parallel to the solid surface. At distances from the wall larger than one fibre length the fibres performed a tumbling motion in the flow-gradient plane in what appeared to be Jeffery-like orbits. Closer to the wall a difference was found between fibres of aspect ratio  $r_p = 10$  and 40. The longer fibres of  $r_p = 40$  kept their orientation, aligned with the flow, also in the near wall region. For the shorter fibres the orientation shifted gradually, to orientations closer to the vorticity axis, when the distance from the wall was decreased. In the very proximity to the wall the fibres were aligned with the vorticity, perpendicular to the direction of the flow. Another distinction, most likely related to the fibre orientation, was seen in the wall normal concentration profile. Due to sedimentation effects fibres accumulated in the near wall region. For fibres of  $r_p = 10$  a peak in concentration was found at the wall, while for  $r_p = 40$  the maximum concentration was found approximately half a fibre length from the wall. It is previously known that a fibre can interact with the wall in what is referred to as a "pole vaulting" motion away from the wall. It is suggested, as a likely explanation to the location of the maximum concentration, that fibres of  $r_p = 40$  perform this motion, while fibres of  $r_p = 10$  do not.

In another experiment the surface of the wall was modified with ridges. For fibres of  $r_p = 10$  there were no longer any fibres oriented perpendicular to the flow direction in the near wall region.

The main application in mind throughout this work is papermaking. The study is considered to be of fundamental character and is not applicable in a direct sense. The difference between the flow situation in the experiments and the paper machine is discussed further.

**Descriptors:** fluid mechanics, fibre orientation, shear flow, fibre suspension, papermaking

## **Preface**

This licentiate thesis in fluid mechanics deals with fibre orientation in shear flows. Particular emphasis is put on flows where the suspended fibres are influenced by a solid surface. The primary application in mind is manufacturing of paper, where shear layers are generated along all the solid surfaces present in the headbox. The thesis is divided into two parts. Part I provides a brief introduction to papermaking as well as an overview of relevant work performed in the area of fibre orientation. Part II consists of three papers that, for consistency, have been adjusted to the format of the thesis.

January 2007, Stockholm

*Allan Carlsson*

# Contents

|  |     |
|--|-----|
| <b>Abstract</b>  | iii |
| <b>Preface</b>   | iv  |
| <b>Part I. Overview and summary</b>                                  | vii |
| <b>Chapter 1. Introduction</b>                                       | 1   |
| 1.1. Paper manufacturing   | 1   |
| 1.2. Fibre orientation   | 1   |
| <b>Chapter 2. Rod-like particles in shear flow</b>                   | 5   |
| 2.1. Fluid motion  | 5   |
| 2.2. Unbounded shear flow  | 6   |
| 2.3. Inertial effects  | 12  |
| 2.4. Wall-bounded shear flow   | 13  |
| 2.5. Summary   | 15  |
| <b>Chapter 3. Fibre orientation in a flow over an inclined plane</b> | 17  |
| 3.1. Experimental setup  | 17  |
| 3.2. Results   | 18  |
| <b>Chapter 4. Relevance for paper manufacturing</b>                  | 21  |
| 4.1. Flow properties   | 21  |
| 4.2. Suspension properties   | 22  |
| <b>Chapter 5. Concluding remarks</b>                                 | 23  |
| <b>Chapter 6. Papers and authors contributions</b>                   | 25  |
| <b>Acknowledgements</b>  | 28  |
| <b>References</b>  | 30  |

|  |           |
|--|-----------|
| <b>Part II. Papers</b>   | <b>33</b> |
| <b>Paper 1. Fibre orientation control related to papermaking</b>   | <b>37</b> |
| <b>Paper 2. Orientation of fibres in a flowing suspension near a plane wall</b>                            | <b>65</b> |
| <b>Paper 3. Evaluation of steerable filters for detection of rod-like particles in flowing suspensions</b> | <b>81</b> |

# Part I

## Overview and summary



## CHAPTER 1

# Introduction

This thesis deals with the orientation of fibres suspended in shear flows, near a solid surface. Rod-like particles in flowing suspensions are present in various applications. The primary application in mind in this work is paper production. Experiments have been performed on fibres suspended in a viscous fluid. Although not applicable, in a direct sense, it is the author's belief that the thesis may provide insights that can be useful for papermaking. For readers, who are not familiar with papermaking and the relevance of fibre orientation, a brief background is given. The primary sources for the text in this chapter is Fellers & Norman (1998) and Gavelin (1990).

### 1.1. Paper manufacturing

The ability to produce paper has its origins in China, where paper was manufactured roughly 2000 years ago. Originally all paper sheets were made by hand in a slow process, whereas today there are machines that produce more than 100,000 tons/year. Although paper as a product has been around for several centuries, all of the physical mechanisms present in the manufacturing process are not fully understood. Thus, the prospects of improving the process are still promising.

Paper consists of a network of fibres, where the most commonly used fibres in manufacturing are cellulose fibres from wood. To produce paper a fibre suspension, a mixture of water and cellulose fibres, with a mass fraction of fibres less than 1% enters a part of the paper machine often referred to as a headbox. The main assignment of the headbox is to transform a pipe flow, with a diameter of about 800 mm, to a uniform jet around 10 mm thick and up to 10 m wide. The jet leaving the headbox impinges on one or two permeable bands called wires. This is followed by large machinery consisting of a press section and a drying section. The primary aim of the press and drying section is to remove the water from the suspension. A schematic of the initial part of a paper machine is shown in figure 1.1.

### 1.2. Fibre orientation

A parameter of relevance for the mechanical properties of a paper sheet is the fibre orientation. A lot of work has been performed concerning fibre orientation

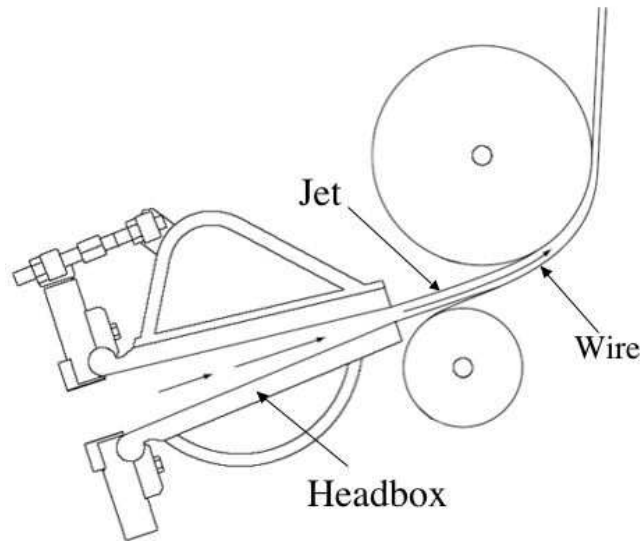


FIGURE 1.1. Schematic of a headbox.

in papermaking. Odell & Pakarinen (2001) made a recent overview on fibre orientation related defects on different scales and their effect on the paper sheet. The majority of the fibres, in the final product, are oriented in the machine direction. This leads to a stronger tensile strength in the machine direction, than in the cross direction. The orientation of the fibres in the paper sheet is determined early in the paper machine. Shortly after the impingement of the jet the fibres create a network and can no longer move in relation to each other.

Several studies have shown that the flow conditions in the headbox are significant for the fibre orientation in the final paper sheet. Due to the streamwise acceleration of the suspension in the headbox the fibres tend to align with the flow direction. Jansson (1998) investigated the effect, on the fibre orientation, of the contraction ratio of the headbox nozzle at minimum shear conditions during dewatering. The anisotropy of the fibre orientation distribution was low at the surfaces, even though the anisotropy around the sheet centre was high. It could be argued that this effect is related to the impingement of the jet, where the initial rate of dewatering is high. Another possible explanation was proposed by Asplund & Norman (2003). Measurements of the fibre orientation were made over the thickness of the jet leaving the headbox. It was shown that, already at this stage of the process, the anisotropy was clearly lower near the surfaces of the jet. This suggests that the low anisotropy, seen at the surfaces

of the paper sheet, are related to the shear layers generated along the solid surfaces in the headbox nozzle.

Another property of interest is the formation, *i.e.* the local mass distribution of fibres, of the paper. One often desires a paper to be as smooth as possible. In an empty headbox nozzle, which can be regarded as a convergent channel, large-scale fluctuations may occur in the flow. This can in turn lead to a poor formation. In order to reduce the problem a set of flexible flow dividers, here referred to as lamellas, are usually implemented in the headbox. At the interface of the suspension and solid surfaces the velocity of the fluid is zero. This leads to a formation of thin layers of shear along the surfaces of the lamellas, where the velocity gradually increases. The hydromechanical term for these shear layers is boundary layers. How fibres behave in shear flows when a solid surface is present is not obvious and is the main theme of this thesis.



## CHAPTER 2

### Rod-like particles in shear flow

In this chapter a review is made of the progress in the field of orientable particles. Extensive work has been done in the field and related areas. In order not to depart too far from the theme of this work some restrictions are introduced.

The fluid in which the particles are suspended is assumed to be Newtonian, *i.e.* the shear stress of the fluid is linearly proportional to the rate of strain. This assumption holds in paper production, where water is the main ingredient. It should be mentioned that when particles are immersed in a Newtonian liquid the properties of the mixture as a whole could show non-Newtonian properties. The study of non-Newtonian fluids is termed rheology. The rheological properties of a suspension generally depend on the orientation of the particles. However, studies concerning the rheology of suspensions are not regarded here, at least not in a rheological sense.

Another restriction is that the effect of Brownian diffusion is considered to be negligible. Brownian motion is particularly significant for suspensions with very small particles. It is convenient to introduce a rotary Peclet number  $Pe = \dot{\gamma}/D$  to characterise the influence of Brownian effects, see for instance Chen & Jiang (1999). In the expression  $\dot{\gamma}$  is the shear rate of the fluid and  $D$  is a rotary diffusivity coefficient dependent on the temperature, viscosity and particle parameters. In the shear layers in a headbox  $Pe \approx 10^{11}$  and thus molecular diffusion is negligible.

#### 2.1. Fluid motion

The motion of an incompressible Newtonian fluid is described by Navier-Stokes equations

$$\frac{\partial \mathbf{u}}{\partial t} + (\mathbf{u} \cdot \nabla) \mathbf{u} = -\frac{1}{\rho} \nabla p + \nu \nabla^2 \mathbf{u} + \mathbf{f} \quad (2.1)$$

$$\nabla \cdot \mathbf{u} = 0, \quad (2.2)$$

where  $\mathbf{u}$  is the fluid velocity,  $t$  is the time,  $p$  is the pressure and  $\mathbf{f}$  is a body force term. The fluid properties, density and kinematic viscosity, is denoted by  $\rho$  and  $\nu$ , respectively. In order to get an indication of the characteristics of a flow a non-dimensional number, referred to as the Reynolds number  $Re = UL/\nu$ , is often introduced. The parameters  $U$  and  $L$  correspond to a, for the particular

flow, characteristic velocity and length scale, respectively. For steady flows where the inertial effects are negligible as compared to effects of viscosity, *i.e.*  $Re \ll 1$ , equation (2.1) is approximately reduced to

$$\frac{1}{\rho} \nabla p = \nu \nabla^2 \mathbf{u} + \mathbf{f}. \quad (2.3)$$

Flows that are described by equation (2.3) are generally called Stokes flows.

## 2.2. Unbounded shear flow

### 2.2.1. Single particles

The motion of a solid ellipsoid, with a surface defined by  $x'^2/a^2 + y'^2/b^2 + z'^2/c^2 = 1$ , suspended in a simple shear flow, was computed analytically by Jeffery (1922). For the case where  $b = c$ , *i.e.* a spheroid, the solutions are

$$\dot{\phi} = -\frac{\dot{\gamma}}{r_e^2 + 1} (r_e^2 \sin^2 \phi + \cos^2 \phi) \quad (2.4)$$

$$\dot{\theta} = \left( \frac{r_e^2 - 1}{r_e^2 + 1} \right) \frac{\dot{\gamma}}{4} \sin 2\phi \sin 2\theta, \quad (2.5)$$

where  $\dot{\gamma}$  is the shear rate and  $r_e = a/b$  is the ellipsoidal aspect ratio. Jeffery's equations are valid for both prolate spheroids ( $r_e > 1$ ) and oblate spheroids ( $r_e < 1$ ), but since the main focus of this study concerns rod-like particles only the motion of prolate spheroids will be considered. For a simple shear, with a velocity defined by  $\mathbf{u} = \dot{\gamma} y \mathbf{e}_x$ , the angle  $\phi$  is taken from the flow direction  $x$  to the projection of the  $x'$ -axis in the  $xy$ -plane and  $\theta$  is the angle from the vorticity axis  $z$  to  $x'$ . The coordinate system is illustrated in figure 2.1.

Equations (2.4) and (2.5) are valid for conditions in which the particle Reynolds number  $Re_L = (\dot{\gamma} L^2)/\nu \ll 1$ , where  $L$  is typically  $a$  or  $b$ . Directly from the equations it is seen that the angular velocities  $\dot{\phi}$  and  $\dot{\theta}$  depend linearly with the shear rate. The spheroid will rotate in closed orbits with a period

$$T = \frac{2\pi}{\dot{\gamma}} \left( \frac{r_e^2 + 1}{r_e} \right). \quad (2.6)$$

If equations (2.4) and (2.5) are integrated with respect to time they may be rewritten to

$$\cot \phi = -r_e \cot \left( \frac{2\pi t}{T} + \phi_0 \right) \quad (2.7)$$

$$\tan \theta = \frac{C r_e}{(r_e^2 \sin^2 \phi + \cos^2 \phi)^{1/2}}, \quad (2.8)$$

where  $C$  is the orbit constant and  $\phi_0$  is the initial value of  $\phi$ . A number of possible orbits are illustrated in figure 2.2, for  $r_e = 40$ . For  $C = 0$  the spheroid is oriented with its major axis aligned with the vorticity axis and it rotates around this axis with a constant angular velocity  $\dot{\gamma}/2$ . As  $C$  approaches infinity the major axis of the spheroid will be located in the flow-gradient plane,

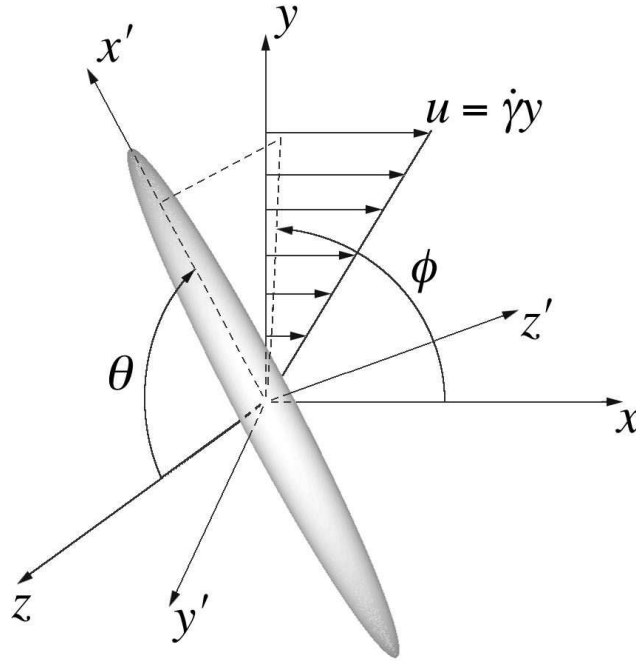


FIGURE 2.1. Coordinate system.

aligned with the flow for most of the time to occasionally, with a period of  $T/2$ , flip around the vorticity axis. In the remainder of this text, when discussing the orientation of a spheroid, or another elongated particle, the major axis is implied.

Bretherton (1962) extended Jeffery's analysis to be valid for almost any body of revolution, with a fore-aft symmetry. As a result equations (2.4) - (2.8) are valid also for particles of cylindrical shape, provided that an equivalent ellipsoidal axis ratio is found. For certain very long bodies, the orbits will however be different from those of Jeffery.

The orbit that a spheroid will undergo is defined by  $C$  and the spheroid will, according to the equations, follow this orbit for an indefinite time. Jeffery also calculated the average rate of dissipation of energy during the periodic motion and came up with a "minimum energy" hypothesis. Accordingly, the spheroid will tend to perform the motion that results in the minimum average dissipation of energy. For prolate spheroids this motion is given by  $C = 0$ .

In an attempt to verify Jeffery's minimum energy hypothesis Taylor (1923) was the first to perform an experimental study on spheroids, in a flow between two concentric cylinders. Prolate spheroids of  $r_e < 3$  aligned with the axis

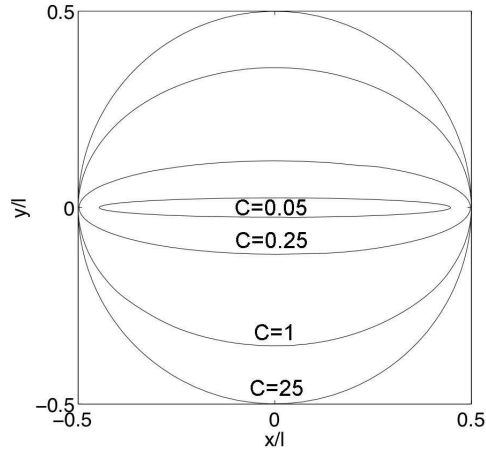


FIGURE 2.2. The path of one of the end points of a cylindrical particle, of aspect ratio  $r_e = 40$ , rotating in Jeffery orbits. The path is projected on the  $xy$ -plane for various values of  $C$ .

of vorticity as suggested by Jeffery. The process was gradual and before the final state was reached Taylor observed the oscillating motion described by Jeffery, although no measurements were made to analyse the orbits. A study on a similar experimental setup was performed by Binder (1939) on cylindrical particles of varying aspect ratios  $r_p = l/d$ , where  $l$  and  $d$  is the length and diameter of the cylinder, respectively. For shorter particles than  $r_p \approx 15$  the particles finally reached a state where orbits corresponding to  $C = 0$  were observed. For longer particles orbits of large  $C$  were observed, thus not in consistency with Jeffery's minimum energy hypothesis. Binder suggested that the reason for the discrepancy might lie in the neglect of inertia in Jeffery's analysis.

First to verify Jeffery's equations experimentally were Trevelyan & Mason (1951). The experiments were performed in a Couette apparatus on cylindrical particles<sup>1</sup> with  $r_p$  in the range from 20 to 120. An equivalent aspect ratio was determined by measuring the period of rotation and extract  $r_e$  from (2.6).

A number of analytical studies, under flow conditions in which inertia can be neglected, has been done concerning the force and torque acting on long slender bodies. Cox (1970, 1971) and Tillett (1970) considered the force and torque on bodies of circular cross-section, where Cox also allowed a curvature of the body. A similar work was done by Batchelor (1970) for straight bodies

<sup>1</sup>Although Taylor (1923) performed initial experiments on spheroids, the first measurements on the periodicity of spheroids is not reported until several years later by Anczurowski & Mason (1968). This is probably related to the difficulties of manufacturing spheroids.

with an arbitrary non-circular cross-section. Some years later Keller & Rubinow (1976) investigated the force per unit length on a slender body of circular cross-section. In addition to earlier studies the body was also permitted to twist and dilate. Yet another theoretical work was presented by Geer (1976), where there were no restrictions on the flow other than the fulfillment of Stokes equations. Chwang & Wu (1975) presented a number of exact solutions to Stokes flow problems, including flows past prolate spheroids. For a spheroid suspended in a paraboloidal flow governed by  $\mathbf{u} = K(y^2 + z^2)\mathbf{e}_x$ , where  $K$  is a constant of unit [1/ms], Chwang (1975) concluded that the motion of a spheroid could be described by Jeffery's equations with the shear rate evaluated at the centre of the spheroid. As a consequence of this result, sufficiently small spheroids will move in Jeffery orbits also in Poiseuille flow.

Goldsmith & Mason (1962) performed an experimental study with single rods of cylindrical shape in a flow satisfying Stokes equations. The particles were suspended in a circular Poiseuille flow, *i.e.* with a velocity governed by

$$u(r) = \frac{2Q}{\pi R^4}(R^2 - r^2), \quad (2.9)$$

where  $Q$  is the volume rate of flow,  $r$  is the radial distance from the center of the tube and  $R$  is the radius of the tube. The motion of the rods was in good agreement with Jeffery's solutions, provided that an equivalent aspect ratio was found from equation (2.6), with  $\dot{\gamma}$  taken at the  $r$ -position where the centre of the rod was located.

As already mentioned work has been conducted in order to find the equivalent ellipsoidal aspect ratio for cylindrical particles. This has been studied by Trevelyan & Mason (1951) and Goldsmith & Mason (1962), but also by Anczurowski & Mason (1968). Anczurowski & Mason (1968) measured the periodical orbits of spheroids in a Couette flow. The results were in good agreement to Jeffery's equations. In the same study experiments were conducted on cylindrical particles mainly in order to determine the point of transition from discs ( $r_e < 1$ ) to rods ( $r_e > 1$ ), corresponding to orbits of oblate and prolate spheroids, respectively. The transition was found to take place at a particle aspect ratio of  $r_p = 0.86$ . A second result from the study was that  $r_p = r_e$  when  $r_p = 1.68$ . Experiments were also carried out on particles of  $r_p$  up to 100 and the equivalent  $r_e$  was calculated. One of the key results found by Cox (1971) was an expression relating  $r_p$  of cylindrical bodies to an equivalent  $r_e$

$$r_e = \left(\frac{8\pi}{3L}\right)^{1/2} r_p (\ln r_p)^{-1/2}, \quad (2.10)$$

where  $L$  is a constant dependent on the shape of the blunt ends of the body. Cox compared equation (2.10) to the experiments conducted on cylindrical particles by Anczurowski & Mason and concluded that  $L = 5.45$  resulted in the best fit. Equation (2.10) is derived for long bodies and is valid only for large  $r_p$ . Another expression relating  $r_p$  of cylindrical particles to an equivalent  $r_e$

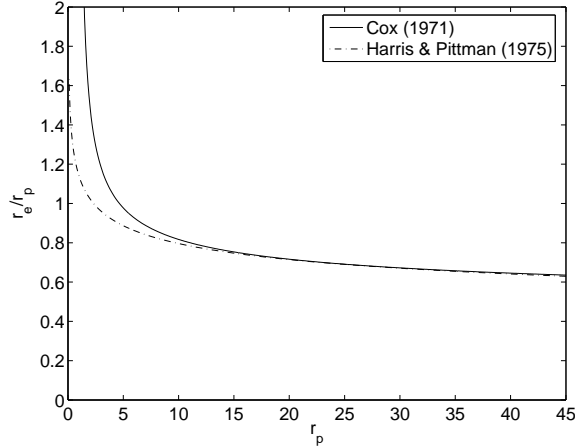


FIGURE 2.3. Equivalent ellipsoidal aspect ratio  $r_e$  of cylindrical particles with aspect ratio  $r_p$ .

was deduced by Harris & Pittman (1975). Experiments were made in a plane Couette flow, which resulted in

$$r_e = 1.14r_p^{0.844}. \quad (2.11)$$

The expression was reported to agree with the measurements of Trevelyan & Mason, within 5%, down to  $r_p = 1$ . In figure 2.3 equation (2.11) by Harris & Pittman is shown and compared with equation (2.10) by Cox.

### 2.2.2. Particle interactions

In suspensions of rod-like particles, the particles can interact through fluid stresses or direct mechanical contact. In this text  $nl^3$ , the number of fibres within a volume  $l^3$ , is used to denote the concentration of the suspension. A common procedure to get an indication of how frequent particle interactions are is to consider different regimes of concentration. For concentrations of  $nl^3 \ll 1$ , where particle interactions can be neglected, the suspension is called dilute. The regime  $nl^3 \gg 1$  and  $nl^2d \ll 1$  is called semi-dilute and is dominated by hydrodynamic interactions. Mechanical contact becomes relevant in the semi-concentrated regime where  $nl^2d = O(1)$ .

In the dilute regime the results discussed in the previous section are valid. However, it turns out that Jeffery's equation provide a good approximation also for higher concentrations. Koch & Shaqfeh (1990) derived a correction to the rate of rotation, due to hydrodynamic interaction in a semi-dilute fibre suspension. For a Jeffery rotation rate of  $O(\dot{\gamma})$  in a dilute suspension the

correction was shown to be  $O(\dot{\gamma}/\ln(1/c_v))$  in the semi-dilute regime, where  $c_v$  is the volume fraction of fibres.

Mason & Manley (1956) studied the motion of cylindrical particles in a shear flow. Experiments were performed on low concentration suspensions ( $nl^3 < 1$ ) with  $r_p$  in the range between 20 and 120. A drift towards a preferential orientation in the flow direction was seen, for all initially isotropic suspensions. The drift was stronger for larger  $r_p$ . Similar experiments were performed by Anczurowski & Mason (1967). The orbit distribution of rods of  $r_p = 18.4$  was investigated for concentrations in the range  $nl^3 = 0.016$  to  $0.52$ . For  $nl^3 < 0.1$  the distribution of orbits was independent of concentration. About 50% of the fibres rotated in orbits with  $C < 0.2$ . Note that this does not necessarily contradict a preferential direction near the flow direction. When moving in Jeffery orbits, the fibres spend most of their time nearly aligned with the  $xz$ -plane. This means that, in this phase of the orbit, for  $C = 0.2$  and  $r_e \approx 13$ , the fibres are oriented only about 20 degrees from the flow direction. Thus, in the experiments by Anczurowski & Mason (1967), more than 50% of the fibres will spend most of their time oriented less than 20 degrees from the flow direction. Although only low concentrations were under study a small shift in the direction of orbits corresponding to higher values of  $C$  was seen when the concentration was increased.

Stover, Koch & Cohen (1992) performed experiments on index of refraction matched suspensions in order to visualise suspensions in the semi-dilute regime. The experiments were done in a cylindrical Couette apparatus on suspensions with  $r_p = 16.9$  and  $31.9$  and concentrations between  $nl^3 = 1$  and  $45$ . The particles were reported to rotate around the vorticity axis in the manner described by Jeffery, also for the highest concentration. At small concentrations lower values of  $C$  was favoured, but with an increase of concentration a more uniform  $C$ -distribution was found. Recalling the results of Anczurowski & Mason (1967) this indicates that the shift towards a more preferential orientation in the flow direction, with increasing concentration, continues also in the semi-dilute regime.

At higher concentrations, in the semi-concentrated regime, Sundararajakumar & Koch (2005) performed dynamic simulations. In the study hydrodynamic interactions were neglected and only interactions due to direct mechanical contact were included. It was concluded that collision between fibres caused them to flip more frequently. Experiments on fibre suspensions of  $r_p \geq 50$ , with concentrations between  $nl^2d = 0.2$  and  $3$ , were conducted by Petrich, Koch & Cohen (2000). In consistency with Sundararajakumar & Koch the period of rotation was shorter than the period predicted by Jeffery. At  $nl^2d = 0.2$  the period was about 20% smaller than the period given by equation (2.6). However, when the concentration was increased the period returned to values close to the dilute result. The fibre orientation was also considered. With an increasing

concentration the distribution of orbits shifted slightly towards smaller values of  $C$ .

### 2.3. Inertial effects

It has been previously mentioned that the result of Binder (1939), where fibres of large  $r_p$  were found non-consistent with Jeffery's minimum energy hypothesis, could be due to inertial effects. Otherwise, up to now the flows under study have been assumed to be free from inertia, *i.e.* the particle Reynolds number  $Re_l$  has been small. In many applications the term  $(\mathbf{u} \cdot \nabla)\mathbf{u}$  is not negligible in equation (2.1). Equation (2.3) will thus not be valid. For instance, in the shear layers along the lamellas in the headbox of a paper machine,  $Re_l$  is typically larger than 250.

An analytical study concerning the inertial effects on long slender bodies was performed by Khayat & Cox (1989). The hydrodynamic force and torque on the body, held fixed in a uniform flow, were derived. For finite Reynolds numbers an orientation dependent non-zero torque was found. As a result a body with fore-aft symmetry, when sedimenting in the vertical direction, rotates to an equilibrium horizontal orientation.

The effect of inertia on a cylinder aligned with the vorticity axis was studied numerically by Ding & Aidun (2000). For low  $Re_{dd} = \dot{\gamma}d^2/\nu$  the motion of the cylinder was in good agreement with Jeffery's analysis. For higher  $Re_{dd}$  the period of rotation was shown to increase and eventually become infinitely large at a sufficiently large  $Re_{dd}$ .

In a recent theoretical study Subramanian & Koch (2005) explored the influence of inertia on the motion of fibres in a simple shear flow. One of the conclusions made in the study is that, for a small but finite  $Re_l$ , fibres drift towards orbits of higher  $C$ , *i.e.*  $C \rightarrow \infty$  as  $t \rightarrow \infty$ . For  $Re_l$  larger than a critical Reynolds number

$$Re_{l,c} = \frac{15 \ln(r_p)}{\pi r_e} \sin^{-2}(\theta), \quad (2.12)$$

the fibres cease to rotate and drift monotonically to the flow-gradient plane. Subramanian & Koch also examined a case where both shear and sedimentation were accounted for. When the force of gravitation align with the gradient direction the evolution of  $C$  is given by

$$\frac{dC}{dt} = \left( \frac{2\pi Re_l}{15 \ln(r_p)} \sin^2(\theta) \cos^2(\phi) - \frac{5}{16 \ln(r_p)} \frac{Re_{sed}^2}{Re_l} \right) C, \quad (2.13)$$

where  $Re_{sed} = U_{sed}l/\nu$  is a Reynolds number based on the sedimentation velocity  $U_{sed}$ . Hence, for sufficiently large  $Re_{sed}$ , as compared to  $Re_l$ , the orbit constant will drift towards zero and finally align with the vorticity axis.

Qi & Luo (2003) numerically investigated the motion of spheroidal particles of  $r_e = 2$ , suspended in simple shear flows for  $0 < Re_l < 467$ , with  $l = 2a$ ,

where  $a$  is the half length of the spheroid. Two transitions in the final rotation state were observed within the studied range of  $Re_l$ . For  $0 < Re_l < Re_{l,1} \approx 205$  there was a drift of  $C$  towards larger values and the spheroid finally rotated in the flow-gradient plane. In an intermediate region  $Re_{l,1} < Re_l < Re_{l,2} \approx 345$ , the mean value of  $\theta$  decreased monotonically with increasing  $Re_l$ . For  $Re_{l,2} < Re_l < 467$  an equilibrium state was found for  $\theta = 0$ , *i.e.* when the spheroid was aligned with the vorticity axis, rotating around its major axis. Notable from this study is that the spheroid never ceased to rotate, although the period increased with  $Re_l$ .

#### 2.4. Wall-bounded shear flow

The analysis by Jeffery were made under the assumption that Stokes equations are valid. Apart from this assumption it was also assumed that there were neither particle interactions nor any wall effects. A few studies have been made concerning the motion of elongated particles in the presence of solid boundaries.

Dabros (1985) calculated numerically the motion of a prolate spheroid, with an aspect ratio  $r_e = 2$ , close to a solid boundary. The spheroid was located in the flow-gradient plane, *i.e.* far away from the wall the motion would be described by Jeffery's equations with  $C$  approaching infinity. At large distances from the wall the angular velocity  $\dot{\phi}$  of the spheroid coincided with the solution of Jeffery. Near the wall, at a distance of  $y/a = 1.05$ , where  $y$  is the distance from the wall to the particle centre and  $a$  is the half length of the spheroid, the angular velocity of the spheroid was smaller. This was in particular seen in the phase of the orbit when the spheroid was oriented parallel to the wall, *i.e.*  $\phi = 0$ .

Hsu & Ganatos (1989, 1994) calculated the hydrodynamic force and torque on an arbitrary body of revolution, suspended in a shear flow, with a varying orientation angle relative to a solid wall. The solution was used in order to compute the motion of a prolate spheroid, at distances from the wall down to  $y/a = 1.1$ . As in the study by Dabros the spheroid was fixed in the flow-gradient plane. The spheroid underwent a periodic tumbling motion similar to the motion described by Jeffery, but also oscillated periodically in the wall normal direction. A similar study with similar results was done by Gavze & Shapiro (1997, 1998). Also here a periodic oscillation was found toward and away from the wall at  $y/a = 1$ . It was also concluded that the tumbling motion could be described by Jeffery's equations, but with a larger period closer to the wall. A first-order approximation to account for small particle inertia was introduced. Similar to the case of no inertia, the inertial spheroids performed an oscillatory motion, in the wall normal direction, but simultaneously drifted towards the wall.

Pozrikidis (2005) made a numerical analysis on the motion of a spheroid near a solid wall. This study, was however not restricted to motions where the

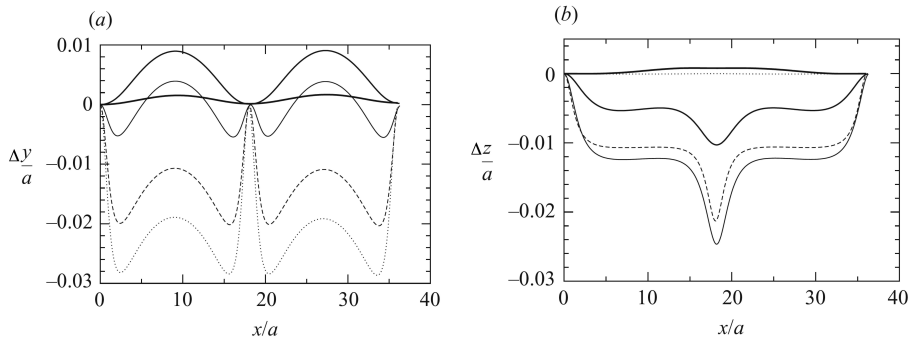


FIGURE 2.4. Projection of the particle centre, of a spheroid of  $r_e = 4$ , in the  $xy$ - and  $xz$ -planes for  $y/a = 1.25$ . The various lines correspond to  $\Phi_0/\pi = 0$  (dotted line),  $\Phi_0/\pi = 0.125$  (dashed line),  $\Phi_0/\pi = 0.25$  (solid line),  $\Phi_0/\pi = 0.375$  (thick solid line) and  $\Phi_0/\pi = 0.46875$  (bold solid line). From Pozrikidis (2005).

particle was fixed in the flow-gradient plane. The initial inclination angle  $\Phi_0$  of the spheroid, to the flow-gradient plane, was varied in the computations. The motion of the particle centre is shown in figure 2.4. Also in this study the particle centre moved periodically in the wall normal direction, when located near the wall. A periodical motion parallel to the vorticity axis was also found when the spheroid was not initially located in the flow-gradient plane nor directed parallel to the vorticity axis. For all initial conditions under study a longer period was found near the wall than far from the wall, where Jeffery's equations were verified. For a particle of  $r_e = 4$  the period increased with approximately 10%, at a distance from the wall of  $y/a = 1.25$ , for any initial angle to the flow-gradient plane.

An experimental study in pressure-driven flow between two solid walls was performed by Stover & Cohen (1990). A special device made it possible to suspend single fibres of  $r_p = 12$  and adjust them to a desired position and orientation. For distances from the wall larger than one fibre length Jeffery's equations were verified for small and high values of  $C$ . Closer to the wall than one fibre length the motion was still periodic, but with a longer period than would be predicted by the shear rate. This trend was seen independent of the value of  $C$ . Furthermore, an interaction with the wall was found for fibres with a large  $C$ , located closer to the wall than half a fibre length. In what was referred to as a "pole vaulting" motion, the fibre moved away from the wall to a point where the centre of mass of the fibre was located at approximately  $y = l/2$ .

Another experimental study on the wall effect was conducted by by Moses, Advani & Reinhardt (2001). The experiments were made in a simple shear flow. The fibres were suspended one at a time, oriented perpendicular to the flow direction, in the flow-gradient plane. For distances at greater distances from the wall than one fibre length Jeffery's equations were verified. Closer to the wall the motion could still be described by Jeffery's equations if an increased effective shear rate was used. Notable is that according to equation (2.6) this would result in a shorter period, thus inconsistent with the other reviewed studies.

The orientation of fibres in a shear flow, near a solid wall, was studied by Holm (2005). A fibre suspension was flowing down an inclined wall. Far upstream from the position where the measurements were made the suspension was accelerated, in the flow direction, to align the fibres with the flow. Experiments were performed on suspensions with aspect ratios between  $r_p = 10$  and 40 and the orientation  $\beta$  in a plane parallel to the wall was analysed. For small  $r_p$  a significant amount of the fibres were oriented perpendicular to the flow direction.

## 2.5. Summary

Several studies have been done in the field of fibre orientation. In particular for unbounded shear flows where the particle motion given by Jeffery's equations have been verified both numerically and experimentally. Accordingly an elongated particle, with a fore-aft symmetry, will move in closed orbits, referred to as Jeffery orbits. In Jeffery's analysis no account is taken for wall effects or particle interactions. Furthermore, Stokes equations are fulfilled, thus removing inertia from the problem.

Experimental studies on suspensions, where particle interactions can not be neglected, has yielded a drift towards higher values of the orbit constant  $C$ . This has been seen for concentrations in the semi-dilute regime. However, for even higher concentrations, in the semi-concentrated regime, Petrich, Koch & Cohen (2000) reported a drift towards lower values of  $C$ . Notable from all these studies are that the particles have been rotating around the vorticity axis in a motion similar to that described by Jeffery.

For flows where inertia is not negligible, relatively little work has been done, on freely suspended particles. For a small but finite  $Re_l$  Subramanian & Koch (2005) and Qi & Luo (2003) reported a drift towards higher values of  $C$ . Subramanian & Koch predicted that for sufficiently large  $Re_l$  the fibre would stop rotating, whereas according to Qi & Luo the fibres never cease to rotate, although the period of the motion do increase for larger  $Re_l$ . Furthermore, Qi & Luo found a second transition towards a preferential orientation. For  $Re_l > 345$  the fibres drifted towards lower values of  $C$ . The only experimental study under review, suggesting that inertia might be of significance, is the

work of Binder (1939). Binder varied the aspect ratio and reported a final state, corresponding to a large value of  $C$ , for sufficiently long fibres.

From numerical studies on the wall effect it has been concluded that the mass centre of the particle will oscillate in the wall normal direction as well as in the direction parallel to the vorticity axis. A longer period, than what would be expected from the shear rate, has been found close to the wall. This was also found experimentally by Stover & Cohen (1990), although a contradicting result was reported by Moses *et al.* (2001). In none of the reviewed studies has there been any discussion concerning a preferential value of  $C$  due to the presence of the wall.

## CHAPTER 3

### Fibre orientation in a flow over an inclined plane

In this chapter the author's own contribution to the field of fibre orientation is summarised. A brief overview of the experimental setup and the essential results is reviewed. For a more detailed description the reader is referred to Part II, the paper section of this thesis.

#### 3.1. Experimental setup

On essentially the same experimental setup as Holm (2005), measurements were done by Carlsson, Lundell & Söderberg (2006*a,b*). Fibre suspensions consisting of cellulose acetate fibres suspended in a viscous fluid were studied. A schematic of the setup is shown in figure 3.1. A film of the suspension, with a thickness of  $h \approx 17$  mm, was flowing down an inclined solid surface, thus generating a shear layer. To visualise the fibres in a plane parallel to the wall a CCD-camera was placed underneath the wall.

Two different aspect ratios ( $r_p = 10$  and  $r_p = 40$ ) and two different wall structures were studied. The first wall structure was a smooth surface and the other a structured surface with ridges, oriented 30 degrees to the flow direction.

Image analysis was used in order to determine the orientation and velocity of individual fibres. By placing the camera to capture images in the flow-gradient plane, it was concluded that the velocity of the fibres correlated well with the distance from the solid surface. This together with the velocity, made it possible to determine the distance from the wall of the fibres also in the images captured from underneath the wall. The studied orientation  $\beta$  of the fibres is defined as the angle, in a plane parallel to the wall, taken clockwise from the flow direction.

#### 3.2. Results

For distances further away from the wall than one fibre length, *i.e.*  $y > l$ , the majority of the fibres kept their orientation aligned with the flow ( $\beta = 0$ ), as initially aligned. For fibres of  $r_p = 40$  this was also the dominating orientation of the fibres, in the near wall region. For fibres of  $r_p = 10$  most fibres were oriented in the flow direction at  $y = l$ , but gradually shifted to an orientation close to perpendicular to the flow direction ( $\beta = 90$ ) in the very proximity to

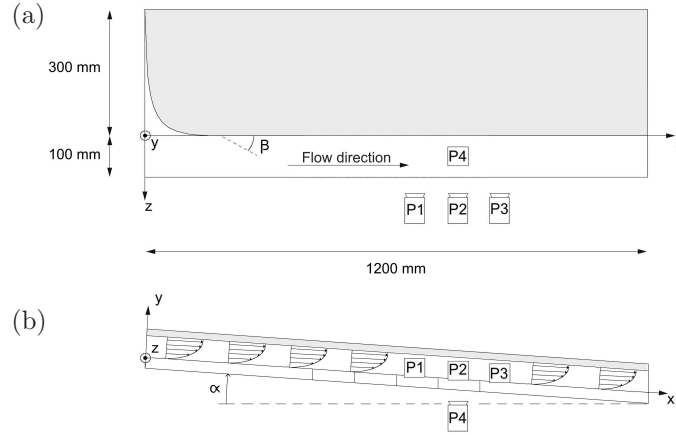


FIGURE 3.1. Schematic figure of the experimental setup from the top (a) and from the side (b).

the wall. In figure 3.2  $F(\beta) = P(B \leq \beta)$ , *i.e.* the probability that a fibre is oriented between  $\beta = 0$  and  $\beta$ , is shown.

Carlsson *et al.* also found a difference in the wall normal concentration distribution between the two aspect ratios under study. Due to gravitational effects fibres accumulated in the near wall region. For  $r_p = 10$  the maximum concentration of fibres was found very close to the wall, while for fibres of  $r_p = 40$  the largest concentration was found at  $y \approx l/2$ . It was suggested that fibres of  $r_p = 40$  were performing the pole vaulting motion described by Stover & Cohen (1990), while fibres of  $r_p = 10$  were not.

The reason for the difference found in the near wall region, between longer and shorter fibres, in the work by Carlsson *et al.* is not perfectly clear. Recalling the results of Subramanian & Koch (2005) it is reasonable to believe that inertial effects could be contributing to the observed discrepancy. The particle Reynolds number in the experiments was  $Re_l \approx 0.01$  and  $0.20$  for  $r_p = 10$  and  $r_p = 40$ , respectively. Putting  $\theta = 90$  in equation (2.12), thus restricted to the flow-gradient plane, results in the corresponding  $Re_{l,c} = 1.38$  and  $0.69$ . Thus,  $Re_l < Re_{l,c}$  for both  $r_p$ . Note that  $Re_{l,c}$  is a lower limit defining where fibres will cease to rotate altogether, according to Subramanian & Koch. A drift towards higher values of  $C$  was reported also for values below  $Re_{l,c}$ . With this in mind, inertial effects could be of significance, for  $r_p = 40$  in particular. Another result of Subramanian & Koch, that could be of relevance, is equation (2.13). In the study by Carlsson *et al.*  $Re_{sed} \ll Re_l$  and although  $C$  will decrease for finite periods, related to certain orientations,  $C \rightarrow \infty$  as  $t \rightarrow \infty$ .

If the mechanism, due to inertia, is present, the fibres will tend to drift toward higher values of the orbit constant. However, if the presence of the

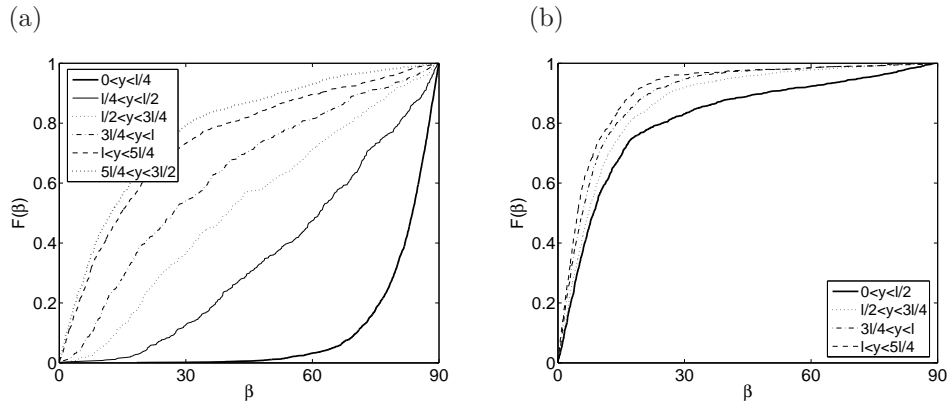


FIGURE 3.2.  $F(\beta)$  for different wall normal distances: (a)  $r_p = 10$  and  $nl^3 = 0.48$ , (b)  $r_p = 40$  and  $nl^3 = 0.48$ . The concentration is here expressed as  $nl^3$  which is the number of fibres within a volume of  $l^3$ . From Carlsson *et al.* (2006b).

wall functions in the other direction, *i.e.* if the wall causes the fibres to drift towards lower values of  $C$ , there would be two mechanisms competing against each other in the near wall region. Assuming for a moment that this is correct, it could be that for fibres of  $r_p = 40$  the inertial drift is stronger, while the drift due to the wall is stronger for  $r_p = 10$ . This would lead to  $C \rightarrow \infty$  for  $r_p = 40$  and  $C \rightarrow 0$  for  $r_p = 10$  as  $t \rightarrow \infty$ . This is a speculative explanation and further studies are required in order to establish if it is correct or not.

Another interesting result from the experiments was found for the case when the solid surface was modified with ridges. For all cases, including fibres of  $r_p = 10$ , the majority of the fibres in the near wall region were oriented in the flow direction.



## CHAPTER 4

### Relevance for paper manufacturing

In Chapter 3 and Part II results from performing experiments, on the orientation of fibres in a wall bounded shear flow, are reported. In this chapter no emphasis is laid on the results of the study, but rather on a brief comparison between the flow and suspension properties in the experiments and in the paper machine.

#### 4.1. Flow properties

The flow in the experiments is a laminar film flow with a film thickness of  $h \approx 17$  mm. The Reynolds number based on  $h$  is  $Re = U_s h / \nu \approx 8$ , where  $U_s$  is the free surface velocity. In the headbox the situation is quite different. The flow can be modeled by a 2D convergent channel, illustrated in figure 4.1. Due to the flow rates the flow in a headbox is to a large extent turbulent. Parsheh (2001) performed experimental investigations of the flow in a 2D convergent channel, with application to headboxes. It was found that towards the end of the contraction the mean velocity profile of an initially turbulent boundary layer approached a self-similar laminar state. The corresponding similarity solution can be found in Schlichting (1979), where the velocity is defined by

$$\frac{u}{U_e} = 3 \tanh^2 \left( \frac{\eta}{\sqrt{2}} + 1.146 \right) - 2, \quad (4.1)$$

where  $U_e$  is the velocity of the fluid outside the boundary layer and  $\eta$  is defined as

$$\eta = y' \sqrt{\frac{U_e}{-(x' - x'_0)\nu}}, \quad (4.2)$$

with the coordinates defined in figure 4.1. The occurrence, that a turbulent boundary layer approach a laminar state, is often termed re-laminarisation and requires a sufficiently strong acceleration. Thus, although the external flow is turbulent, the boundary layers are expected to show a laminar-like behaviour near the exit of the headbox. Note that a self-similar mean flow profile is not sufficient to conclude that the flow is truly laminar in the boundary layer. Studies have shown that parts of the turbulent structures can remain in a re-laminarised boundary layer, see for instance Warnack & Fernholz (1998) and Talamelli, Fornaciari, Westin & Alfredsson (2002). The remaining turbulent

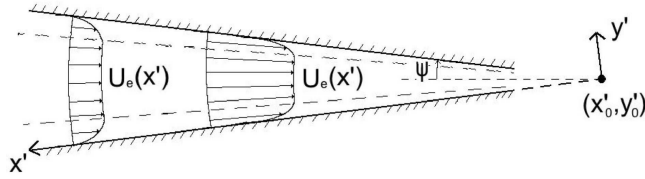


FIGURE 4.1. Two-dimensional convergent channel.

structures may lead to a rapid re-transition to turbulence once there is no longer any acceleration acting on the flow. Acceleration present in the headbox is also expected to affect the fibre orientation. One consequence of the acceleration is that the boundary layer thickness decreases in the flow direction. The order of magnitude of the boundary layer thickness is roughly 1 mm near the end of the lamellas.

#### 4.2. Suspension properties

As already indicated inertial effects play a significant role on the fibre dynamics. For a fibre of length  $l = 0.5$  mm and diameter  $d = 50$   $\mu\text{m}$  the particle Reynolds number based on  $l$  and  $d$  are given by  $Re_l = \dot{\gamma}l^2/\nu$  and  $Re_d = \dot{\gamma}ld/\nu$ , respectively. In the experiments ( $Re_l \approx 0.01$ ,  $Re_d \approx 0.001$ ) and in the headbox ( $Re_l \approx 250$ ,  $Re_d \approx 25$ ) under typical shear rates in respective case. The Reynolds numbers suggest that the fibres will rotate in Jeffery-like orbits in the experimental case, although drifts in the orbit constant may occur due to wall effects, effects of inertia and particle interactions. In the headbox inertial effects are significant and it is unclear whether or not the fibres will rotate in orbits similar to those of Jeffery.

In the experiments the concentration range between  $nl^3 = 0.01$  and 3.82, whereas typical values of  $nl^3$  in the headbox are between 0.5 and 20. Apart from fibres, there are also fillers, fines and various chemical substances present in the paper production. The precise composition depends on the pulp and the specific application, but these additives are likely to have an impact on the fibre motion.

Yet another parameter of significance is the fibre flexibility. In the experiments the fibres are considered to be rigid. However, this is generally not the case in the headbox. Wet pulp fibres are flexible and can bend when suspended in the headbox. The fibre flexibility is different for different pulps. Tam Doo & Kerekes (1981, 1982) developed a method to measure the flexibility of wet fibres. Tests showed that chemical pulps were up to 30 times more flexible than mechanical pulps from the same wood. However, although fibres in mechanical pulps are stiffer than in chemical pulps, they can not be assumed to be rigid.

## CHAPTER 5

### Concluding remarks

Based on the comparison made in Chapter 4 it is clear that a lot of work remains to be done in order to fully understand the situation in a headbox. A first step, before introducing turbulence, is to understand the laminar case thoroughly. It is believed that proceeding in this manner will facilitate understanding of the more complex situation present in the paper machine.

From the review made in Chapter 2 it is concluded that there are not many studies concerning the wall effect on the fibre dynamics. In basically all studies with a solid boundary, inertia has been totally neglected. To the author's knowledge the only exception is the numerical study by Gavze & Shapiro (1998), where a small but finite inertia was included. In fact, there seems to be essentially no experimental studies where effects of inertia are discussed. This is the case also for unbounded shear flows. Experimental studies in the region where the effect of inertia becomes significant ( $Re_l < 1$ ) are thus needed. The experiments would preferably be done in a setup where it is possible to follow the fibres for a long period of time, to be able to detect small drifts in the orbit constant.

In order to understand the fibre motion in the headbox boundary layers more thoroughly two suggestions of topics that need to be addressed are stated.

- The only study found in the region  $Re_l > 1$  is the numerical work by Qi & Luo (2003). Complementary experimental studies are required in this region, recalling that typically  $Re_l > 250$  in the headbox.
- Pulp fibres are generally flexible. Experimental studies concerning the influence of the fibre elasticity are thus required.

More points could obviously be added. For instance, as mentioned in Chapter 4 there are various interactions with different kinds of fillers and chemical substances, depending on the specific pulp. Nevertheless, it is believed that further insights on the two points mentioned are essential if the situation in the headbox is to be understood.



## CHAPTER 6

### Papers and authors contributions

#### **Paper 1**

*Fibre orientation control related to papermaking*

A. Carlsson (AC), F. Lundell (FL) & L. D. Söderberg (DS).

*Accepted for publication in Journal of Fluids Engineering*

The wall effect on the orientation of fibres immersed in a laminar shear flow is investigated. Experiments are performed on two different structures of the solid surface, one smooth and another modified with ridges. The wall is shown to have an effect on the orientation. For fibres of aspect ratio  $r_p = 10$  the fibres are oriented close to perpendicular to the flow direction near the wall, for the smooth surface. When the surface is modified with ridges, this effect is seemingly absent. AC performed the experiments and analysis under supervision of FL and DS. AC, FL and DS wrote the paper jointly. Parts of these results have been presented at (i) ASME Joint U.S.-European Fluids Engineering Summer Meeting, Miami, FL, USA 2006, (ii) Euromech Fluids Mechanics Conference 6, Royal Institute of Technology, Stockholm 2006 and (iii) Nordic Rheology Conference, Royal Institute of Technology, Stockholm 2006.

#### **Paper 2**

*Orientation of fibres in a flowing suspension near a plane wall*

A. Carlsson, F. Lundell & L. D. Söderberg.

The orientation of fibres flowing over a solid surface is studied experimentally. Measurements are performed on two different aspect ratios,  $r_p = 10$  and 40. For fibres of  $r_p = 40$  the majority of the fibres are oriented in the flow direction, as initially aligned, independent of the wall-normal position. For  $r_p = 10$  the orientation shifts gradually, from being nearly aligned with the flow for distances from the wall larger than one fibre length, to being oriented close to perpendicular to the flow direction at the wall. AC performed experiments and analysis under supervision of FL and DS. AC, FL and DS wrote the paper jointly.

### **Paper 3**

*Evaluation of steerable filters for detection of rod-like particles in flowing suspensions*

A. Carlsson, F. Lundell & L. D. Söderberg.

A filter within the class of steerable filters is evaluated for suitability of detecting fibres in flowing suspensions. The concept of steerable filters is concluded to be an efficient method of finding the position and orientation of fibres. Experiments, analysis and writing were performed by AC under supervision of FL and DS.



## Acknowledgements

The work has been financed by ECOTARGET, an EU-funded research project.

I would especially like to thank my supervisors Dr. Fredrik Lundell, Dr. Daniel Söderberg and Prof. Henrik Alfredsson for their guidance and support during these last two years.

A person I believe have had a significant impact on my work is Dr. Richard Holm, who helped me out during my first two weeks at KTH Mechanics. Richard, you gave me a really good start.

For valuable discussions, on my topic as well as unrelated areas, I would like to thank my roommates Gabriele Bellani and Outi Tammisola. Lately, Prof. Fritz Bark and Dr. Anders Dahlkild have also provided me with insights, to the field of fibre dynamics.

Prof. Bo Norman and Krister Åkesson are greatly acknowledged for improving my initially and still lacking knowledge of paper manufacturing. On this topic I would again like to include the already mentioned Dr. Söderberg.

Marcus Gällstedt, Ulf Landén and Timmy Sigfrids have also been valuable to me, by helping me with various practical tasks.

The persons acknowledged above are the ones I feel have had a direct influence on my work. However, there are also others I would like to mention who have meant a lot to me.

Throughout the years I have received the most consistent support from my parents, Gunnar and Ingrid, and my brother David. Other persons who have inspired me, before I started my position at KTH Mechanics, are Hans Moberg and Dr. Lars Söderholm. On this list I could also include Kjell Emmoth who roughly 10 years ago made the field of physics an interesting subject.

Veronica, Mike, Bengt, Ramis, Shiho and Claes are also acknowledged among all other friends at KTH. I would like to mention the Carduelis family who have often greeted me and raised my spirit on my way to work. Hermann

is acknowledged for input of a more philosophical character and finally, I would like to thank you Thang for all the years you have been around.

It is not my intention to leave anyone out from the acknowledgements. However, if I were to mention all the people that have meant something to me in my life, my feeling is that this section would be the dominant part of this thesis. If you, the reader, feel that you have done something for me, you probably have.

## References

- ANCZUROWSKI, E. & MASON, S. G. 1967 The kinetics of flowing dispersions. III. Equilibrium orientations of rods and discs (experimental). *J. Colloid Interface Sci.* **23**, 533–546.
- ANCZUROWSKI, E. & MASON, S. G. 1968 Particle motions in sheared suspensions. XXIV. Rotation of rigid spheroids and cylinders. *Trans. Soc. Rheology* **12** (2), 209–215.
- ASPLUND, G. & NORMAN, B. 2003 Fibre orientation anisotropy profile over the thickness of a headbox jet. In *89th PAPTAC Annual meeting, Montreal, Canada*.
- BATCHELOR, G. 1970 Slender-body theory for particles of arbitrary cross-section in Stokes flow. *J. Fluid Mech.* **44**, 419–440.
- BINDER, R. C. 1939 The motion of cylindrical particles in viscous flow. *J. Appl. Phys.* **10**, 711–713.
- BRETHERTON, F. P. 1962 The motion of rigid particles in a shear flow at low Reynolds number. *J. Fluid Mech.* **14**, 284–304.
- CARLSSON, A., LUNDELL, F. & SÖDERBERG, L. D. 2006*a* Fibre orientation control related to papermaking. *J. Fluids Eng.*, Accepted for publication .
- CARLSSON, A., LUNDELL, F. & SÖDERBERG, L. D. 2006*b* Orientation of fibres in a flowing suspension near a plane wall. To be submitted .
- CHEN, S. B. & JIANG, L. 1999 Orientation distribution in a dilute suspension of fibers subject to simple shear flow. *Phys. Fluids* **11** (10), 2878–2890.
- CHWANG, A. T. 1975 Hydrodynamics of low-Reynolds-number flow. Part 3. Motion of a spheroidal particle in quadratic flows. *J. Fluid Mech.* **72**, 17–34.
- CHWANG, A. T. & WU, T. Y.-T. 1975 Hydrodynamics of low-Reynolds-number flow. Part 2. Singularity method for Stokes flows. *J. Fluid Mech.* **67**, 787–815.
- COX, R. G. 1970 The motion of a long slender body in a viscous fluid. Part 1. General theory. *J. Fluid Mech.* **44**, 791–810.
- COX, R. G. 1971 The motion of a long slender body in a viscous fluid. Part 2. Shear flow. *J. Fluid Mech.* **45**, 625–657.
- DABROS, T. 1985 A singularity method for calculating hydrodynamic forces and particle velocities in low-Reynolds-number flows. *J. Fluid Mech.* **156**, 1–21.
- DING, E.-J. & AIDUN, C. K. 2000 The dynamics and scaling law for particles suspended in shear flow with inertia. *J. Fluid Mech.* **423**, 317–344.

- FELLERS, C. & NORMAN, B. 1998 *Pappersteknik*. KTH, Stockholm, Sweden.
- GAVELIN, G. 1990 *Papperstillverkning*. Sveriges Skogsindustriförbund.
- GAVZE, E. & SHAPIRO, M. 1997 Particles in a shear flow near a solid wall: Effect of nonspherity on forces and velocities. *Int. J. Multiphase Flow* **23** (1), 155–182.
- GAVZE, E. & SHAPIRO, M. 1998 Motion of inertial spheroidal particles in a shear flow near a solid wall with special application to aerosol transport in microgravity. *J. Fluid Mech.* **371**, 59–79.
- GEER, J. 1976 Stokes flow past a slender body of revolution. *J. Fluid Mech.* **78** (3), 577–600.
- GOLDSMITH, H. L. & MASON, S. G. 1962 The flow of suspension through tubes I. Single spheres, rods and discs. *J. Colloid Sci.* **17**, 448–476.
- HARRIS, J. B. & PITTMAN, J. F. T. 1975 Equivalent ellipsoidal axis ratios of slender rod-like particles. *J. Coll. Interf. Sci.* **50** (2), 280–282.
- HOLM, R. 2005 Fluid mechanics of fibre suspensions related to papermaking. PhD thesis, Royal Institute of Technology, Stockholm, Sweden.
- HSU, R. & GANATOS, P. 1989 The motion of a rigid body in viscous fluid bounded by a plane wall. *J. Fluid Mech.* **207**, 29–72.
- HSU, R. & GANATOS, P. 1994 Gravitational and zero-drag motion of a spheroid adjacent to an inclined plane at low Reynolds number. *J. Fluid Mech.* **268**, 267–292.
- JANSSON, M. 1998 Fibre orientation anisotropy - variations in the z-direction (in Swedish). MSc thesis, Royal Institute of Technology, Stockholm, Sweden.
- JEFFERY, G. B. 1922 The motion of ellipsoidal particles immersed in a viscous fluid. *Proc. Roy. Soc. London A* pp. 161–179.
- KELLER, J. B. & RUBINOW, S. I. 1976 Slender-body theory for slow viscous flow. *J. Fluid Mech.* **75**, 705–714.
- KHAYAT, R. E. & COX, R. G. 1989 Inertia effect on the motion of long slender bodies. *J. Fluid Mech.* **209**, 435–462.
- KOCH, D. L. & SHAQFEH, E. S. G. 1990 The average rotation rate of a fibre in the linear flow of a semidilute suspension. *Phys. Fluids A* **2**, 2093–2102.
- MASON, S. G. & MANLEY, R. S. J. 1956 Particle motions in sheared suspensions: Orientation and interaction of rigid rods. *Proc. Roy. Soc. London A* **238** (1212), 117–131.
- MOSES, K. B., ADVANI, S. G. & REINHARDT, A. 2001 Investigation of fiber motion near solid boundaries in simple shear flow. *Rheol. Acta* **40**, 296–306.
- ODELL, M. & PAKARINEN, P. 2001 The complete fibre orientation control and effects on diverse paper properties. In *Tappi Papermakers Conference, Cincinnati*.
- PARSHEH, M. 2001 Flow in contractions with application to headboxes. PhD thesis, Royal Institute of Technology, Stockholm, Sweden.
- PETRICH, M. P., KOCH, D. L. & COHEN, C. 2000 An experimental determination of the stress-microstructure relationship in semi-concentrated fiber suspensions. *J. Non-Newtonian Fluid Mech.* **95**, 101–133.
- POZRIKIDIS, C. 2005 Orbiting motion of a freely suspended spheroid near a plane wall. *J. Fluid Mech.* **541**, 105–114.

- QI, D. & LUO, L. S. 2003 Rotational and orientational behaviour of three-dimensional spheroidal particles in Couette flows. *J. Fluid Mech.* **477**, 201–213.
- SCHLICHTING, H. 1979 *Boundary layer theory*, 7th edn. McGraw-Hill.
- STOVER, C. A. & COHEN, C. 1990 The motion of rodlike particles in the pressure-driven flow between flat plates. *Rheol Acta* **29**, 192–203.
- STOVER, C. A., KOCH, D. L. & COHEN, C. 1992 Observations of fibre orientation in simple shear flow of semi-dilute suspensions. *J. Fluid Mech.* **238**, 277–296.
- SUBRAMANIAN, G. & KOCH, D. L. 2005 Inertial effects on fibre motion in simple shear flow. *J. Fluid Mech.* **535**, 383–414.
- SUNDARARAJAKUMAR, R. R. & KOCH, D. L. 1997 Structure and properties of sheared fiber suspensions with mechanical contacts. *J. Non-Newtonian Fluid Mech.* **73**, 205–239.
- TALAMELLI, A., FORNACIARI, N., WESTIN, K. J. A. & ALFREDSSON, P. H. 2002 Experimental investigation of streaky structures in a relaminarizing boundary layer. *J. Turbulence* **3** (018).
- TAM DOO, P. A. & KEREKES, R. J. 1981 A method to measure fiber flexibility. *Tappi* **64** (3), 113–116.
- TAM DOO, P. A. & KEREKES, R. J. 1982 The flexibility of wet pulp fibres. *Pulp Paper Can* **83** (2), 37–41.
- TAYLOR, G. I. 1923 The motion of ellipsoidal particles in a viscous fluid. *Proc. Roy. Soc. London A* **103**, 58–61.
- TILLET, J. P. K. 1970 Axial and transverse Stokes flow past slender axisymmetric bodies. *J. Fluid Mech.* **44**, 401–417.
- TREVELYAN, J. & MASON, S. G. 1951 Particle motions in sheared suspensions I. Rotations. *J. Colloid Sci.* **6**, 354–367.
- WARNACK, D. & FERNHOLZ, H. H. 1998 The effects of a favourable pressure gradient and of the Reynolds number on an incompressible axisymmetric turbulent boundary layer. Part 2. The boundary layer with relaminarization. *J. Fluid Mech.* **359**, 357–381.

**Part II**

**Papers**



# Paper 1



# Fibre orientation control related to papermaking

By Allan Carlsson<sup>†</sup>, Fredrik Lundell<sup>†</sup> & L. Daniel Söderberg<sup>†,‡</sup>

<sup>†</sup>Linné Flow Centre, KTH Mechanics, SE - 100 44 Stockholm, Sweden

<sup>‡</sup>STFI-Packforsk AB, SE - 114 86 Stockholm, Sweden

Accepted for publication in Journal of Fluids Engineering

The orientation of fibres suspended in a shear flow flowing over a solid wall has been studied experimentally. The possibility to control this orientation with physical surface modifications, ridges, has also been studied. The fibre suspension was driven by gravity down a slightly inclined glass plate and a CCD-camera was used to capture images of the fibres in the flow. Image analysis based on the concept of *steerable filters* extracted the position and orientation of the fibres in the plane of the image. From these data, the velocity of the fibres was determined. When viewing the flow from the side, the velocity of the fibres at different heights was measured and found to agree with the theoretical solution for Newtonian flow down an inclined plate. Moving the camera so that the flow was filmed from below, the orientation and velocity of fibres in the plane parallel to the solid surface was determined. The known relationship between the velocity and the wall normal position of the fibres made it possible to determine the height above the plate for each identified fibre. Far away from the wall, the fibres were aligned with the flow direction in both cases. In a region close to the smooth plate surface the fibres oriented themselves perpendicular to the flow direction. This change in orientation did not occur when the surface structure was modified with ridges.

---

## 1. Introduction

The present work is part of a larger undertaking aimed at understanding and controlling the flow physics involved in papermaking. When paper is produced, a fibre suspension consisting of cellulose fibres suspended in water is used. The suspension, with a mass concentration typically below 1%, enters a nozzle, usually called a headbox, through a pipe with a diameter of approximately 800 mm, Fellers & Norman (1998). The main purpose of the headbox is to distribute the suspension evenly across one or between two permeable bands called wires. To do this the pipe-flow entering the headbox is transformed to

a jet with an approximate height of 10 mm and a width of about 10 m. The mechanical properties of the produced paper sheet are strongly coupled to the fibre orientation. Due to the contraction of the headbox, fibres tend to align in the flow direction. This orientation anisotropy is also reflected in the final product.

In order to damp out large-scale velocity fluctuations in the headbox, which can result in a bad formation of the paper, *i.e.* a variation in local mass distribution or basis weight, flexible flow dividers are often implemented in the headbox. These are fixed at the entrance to the nozzle contraction and allowed to adjust according to the flow field. The width of these flow dividers are the same as the width of the nozzle. The flow dividers will henceforth be called lamellas. At the surfaces of the lamellas the no-slip condition is valid, *i.e.* the velocity of the fluid relative to the surfaces is zero. As a result thin shear layers of fluid, *i.e.* boundary layers, will form along the lamella surfaces, where the velocity goes from zero at the surfaces to the velocity of the main stream further out. The aim of the present study is to investigate the physics controlling fibre orientation in a boundary layer close to a solid wall, aiming at understanding how the lamellas influence the fibre orientation and ultimately the properties of the final paper product. It is also of interest to investigate the possibility to use the lamellas as means of controlling the fibre orientation by modifying the structure of the lamella surfaces.

In order to interpret the results of the present study, the concept of Jeffery orbits will be used, *i.e.* the motion of a solitary ellipsoid suspended in a laminar simple shear flow. The equations of motion for the ellipsoid has been solved theoretically by Jeffery (1922) and the resulting expressions, frequently referred to as Jeffery's equations, are

$$\dot{\phi} = -\frac{\dot{\gamma}}{r_e^2 + 1}(r_e^2 \sin^2 \phi + \cos^2 \phi) \quad (1)$$

$$\dot{\theta} = \left(\frac{r_e^2 - 1}{r_e^2 + 1}\right) \frac{\dot{\gamma}}{4} \sin 2\phi \sin 2\theta, \quad (2)$$

where  $\phi$  is the angle of the particle projection in the flow-gradient plane with respect to the streamwise direction, figure 1. The angle of the particle with respect to the vorticity axis is defined as  $\theta$ . The aspect ratio, *i.e.* the length to diameter ratio of the ellipsoid, is denoted  $r_e$  and  $\dot{\gamma}$  is the shear rate. The dots over the two angles  $\phi$  and  $\theta$ , represent differentiation with respect to time. The ellipsoid will remain in its initial orbit, which is defined by the initial conditions. The motion is periodic with a period

$$T = \frac{2\pi}{\dot{\gamma}} \left( \frac{r_e^2 + 1}{r_e} \right). \quad (3)$$

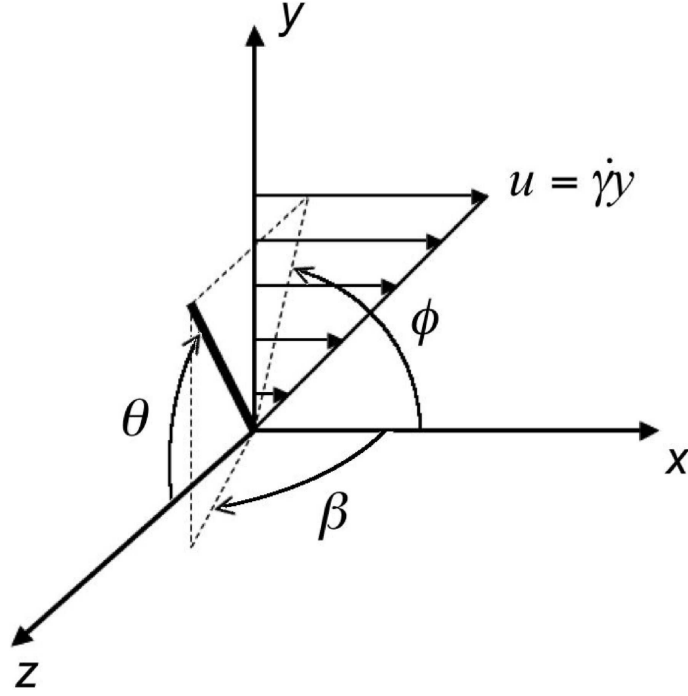


FIGURE 1. Coordinate system.

Integration of equations 1 and 2 with respect to time yields

$$\tan \phi = \frac{1}{r_e} \tan \left( -\dot{\gamma}t \frac{r_e}{r_e^2 + 1} + \tan^{-1}(r_e \tan \phi_0) \right) \quad (4)$$

$$\tan \theta = \frac{Cr_e}{(r_e^2 \sin^2 \phi + \cos^2 \phi)^{1/2}}, \quad (5)$$

where  $C$  is the so called orbit constant and  $\phi_0$  is the initial value of  $\phi$ .

Even though the original derivation of Jeffery's equations relied on the assumption of ellipsoidal particles, it has been shown that it is possible to extend Jeffery's equations to be valid for any body with a fore-aft symmetry, provided that an equivalent aspect ratio is used, Bretherton (1962). In particular, the equivalent aspect ratio for a cylindrical fibre is

$$r_e = 1.24r_p(\ln r_p)^{-1/2}, \quad (6)$$

where  $r_p$  is the aspect ratio of the cylindrical fibre and  $r_e$  is the equivalent aspect ratio to be used in Jeffery's equations, see Cox (1971).

Some examples of Jeffery orbits are shown in figure 2. The orbits are calculated for an equivalent aspect ratio  $r_e = 8.17$ , which corresponds to a

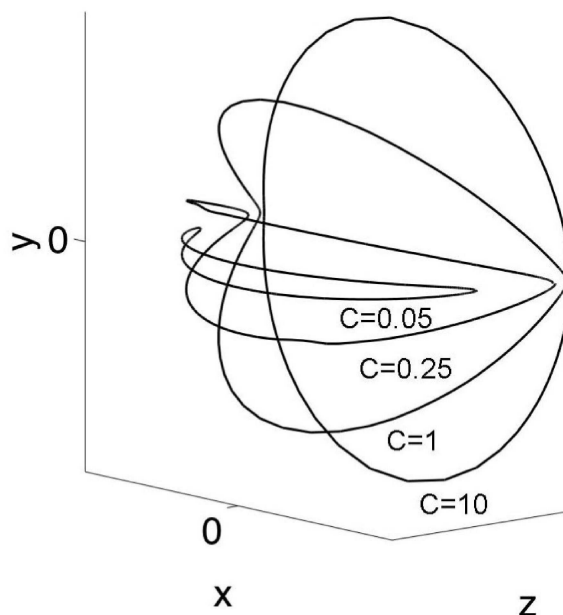


FIGURE 2. Jeffery orbits for different values of the orbit constant  $C$  and  $r_e = 8.17$ .

cylindrical fibre with aspect ratio 10 as used in the present study. The flow is in the  $x$ -direction and the shear is in the  $y$ -direction. Four different orbits are shown in figure 2. The orbits are shown as the path of a fibre end-point. For high values of  $C$  the fibre spend most of its time oriented close to the flow direction. Occasionally, with a period of  $T/2$ , it flips over 180 degrees around the vorticity axis. As the value of  $C$  is lowered the amplitude of the motion in the  $y$ -direction decreases. For very low values of  $C$  the fibre is almost parallel to the  $xz$ -plane, oriented perpendicular to the flow direction.

Jeffery's equations have been verified by several researchers, including Moses, Advani & Reinhardt (2001), Taylor (1923) and Binder (1939), but do not account for fibre-fibre interactions or wall effects. The wall effect has been investigated both experimentally by Moses *et al.* and theoretically by Pozrikidis (2005). For elongated particles, a good agreement of Jeffery's equations was found, in the study by Moses *et al.*, for distances from the wall larger than one fibre-length, whereas an increased rate of rotation was found closer to the wall. The spatial orbit was not considerably changed.

At higher concentrations, it has been shown by Koch & Shaqfeh (1990) that the correction to the  $O(\dot{\gamma})$  rotation rate is  $O(\dot{\gamma}/\ln(1/c_v))$  where  $c_v$  is

the volume fraction of the fibres. For a concentration of 1% this correction is  $O(20\%)$ .

Initially in this paper, the experimental setup and evaluation methods are described followed by a discussion regarding why the present experiments, performed at low velocities in a highly viscous fluid, are relevant for papermaking. Thereafter the results are presented and discussed followed by conclusions. In the paper we present measurements of the previously discarded fibre orientation in the  $xz$ -plane, and in particular the effect of a wall including the possibility to manipulate the orientation by modifying the surface structure of the wall.

## 2. Experimental setup & analysing techniques

To create a well-defined shear flow a fibre suspension was allowed to flow down a slightly inclined glass plate. To visualise the flow a CCD-camera has been used, and by analysing the captured images the velocity and orientation of the fibres in the shear flow can be obtained. Below, the flow loop, liquid and fibres are described. Thereafter the image analysis methodology is introduced, which is performed in two steps: (i) detection of the position and orientation of fibres in an image and (ii) determination of the velocity from a triplet of consecutive images. The flow in the apparatus is verified by comparing measured velocity profiles of the fibres with the theoretical profile.

### 2.1. Experimental setup

The experimental setup, illustrated in figure 2, consists of a (1200 x 400) mm<sup>2</sup> glass plate with a thickness of 6 mm. A pivoting acrylic frame with for-aft reservoirs, not shown in the figure, supports the plate. A membrane pump (Dominator P30-ANN) is used to transfer the fluid between the reservoirs. By placing an insert on the glass plate the flow is given an inlet contraction followed by a parallel section of length 1050 mm and width 100 mm. The contraction stretches over a length of 150 mm and has a contraction ratio of four. Due to the acceleration in the contraction the fibres align themselves with the flow direction.

Experiments have been performed using two different surfaces. The first is a smooth surface and the second is a structured surface with ridges oriented 30 degrees counter-clockwise to the flow direction. The ridges were machined in four (100 x 100) mm<sup>2</sup> acrylic plates of height 6 mm. These plates covered the region from  $x = 400$  mm to  $x = 800$  mm. The position and structure of the ridges is illustrated in figure 4, where  $H = 0.5$  mm. In the case of the smooth surface a (1200 x 100) mm<sup>2</sup> acrylic plate of height 6 mm is placed in the flow section on top of the glass plate in order to ensure that the flow situation was similar to the case with ridges.

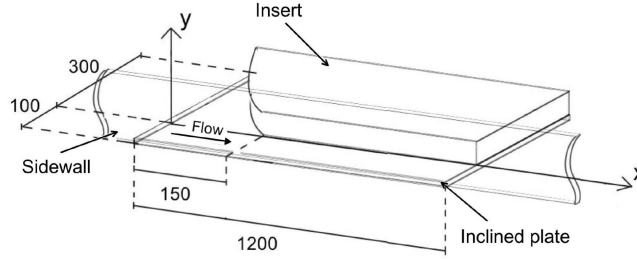


FIGURE 3. Schematic figure of the test section. All lengths are given in mm.

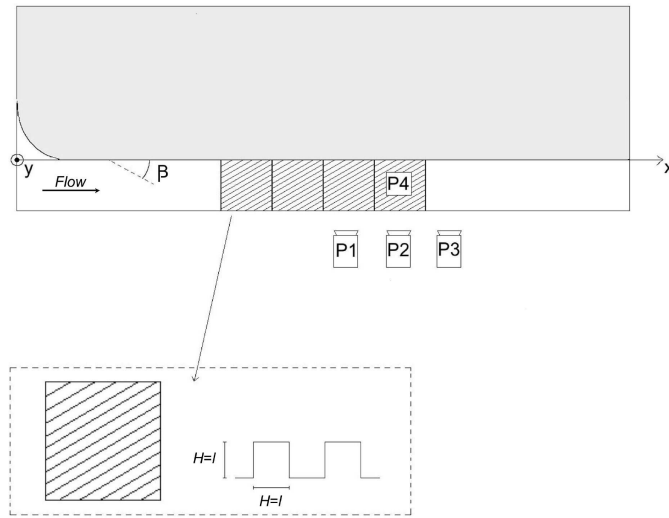


FIGURE 4. Schematic figure illustrating the camera positions for the velocity profile measurements (P1, P2 and P3) and for the fibre orientation studies P4.

## 2.2. Flow situation

The theoretical velocity profile for a Newtonian fluid flowing down an inclined plate is given by

$$u = \frac{g}{2\nu}y(2h - y) \sin \alpha, \quad (7)$$

where  $g$  is the gravitational constant,  $\nu$  is the kinematic viscosity of the fluid,  $h$  is the fluid film thickness and  $\alpha$  is the inclination of the plate with respect

to the horizontal, see for instance Acheson (1990). The distance from the wall,  $y$  in equation 5, stretches from  $y = 0$  at the wall to the surface of the liquid film  $y = h$ . Equation 5 is thus a parabolic expression where the velocity is zero at the wall to gradually increase with the distance to the wall. The highest velocity is found at  $y = h$ , where  $u = U_s$ .

In the experiments a tilt angle of  $\alpha = 2.60 \pm 0.1^\circ$  caused the suspension to form a liquid film along the plate with a thickness of  $17.0 \pm 0.2$  mm. The film thickness was measured to be constant throughout the section between  $x = 650$  mm and  $x = 850$  mm. It can thus be established that there was no global acceleration in the flow. The Reynolds number, based on the film thickness and the velocity at the surface of the film, is defined as

$$\text{Re} = \frac{U_s h}{\nu}. \quad (8)$$

For the highly viscous flow in the experiments  $\text{Re} \approx 8$ .

### 2.3. Fibre suspension

The liquid containing the fibres was a mixture of glycerine and polyethyleneglycol (PEG-400). The temperature of the suspension was  $295.5 \pm 0.5$  K throughout the measurements. For this temperature the kinematic viscosity of the liquid was measured to  $\nu = (383 \pm 10) \cdot 10^{-6}$  m<sup>2</sup>/s and the density to  $\rho_f = 1210 \pm 15$  kg/m<sup>3</sup>.

Cellulose acetate fibres were suspended in the liquid. The length of the fibres was  $l = 0.5$  mm and the diameter was approximately  $d = 50$   $\mu\text{m}$ . The density of the fibres was approximately  $\rho_p = 1300$  kg/m<sup>3</sup>. Since the density of the fibres is higher than the density of the liquid, the fibres will sediment slowly when suspended in the liquid. The suspension was dilute with a volume fraction of fibres  $c_v = 0.004$ . This concentration can be expressed as  $nl^3 = 0.48$ , which is the number of fibres within a volume  $l^3$  ( $n$  is the number density of fibres).

The index of refraction (IR) of the liquid was approximately matched to that of the fibres and the IR of the liquid was measured to  $n = 1.466 \pm 0.002$ . IR matching is a frequently used tool in multiphase flows and has been used in several previous studies of fibre suspensions, see Iso, Koch & Cohen (1995), Petrich, Koch & Cohen (2000), Holm (2005) and Herzhaft & Guazzelli (1999). In order to visualise the fibres 4% were dyed black.

### 2.4. Measuring and analysing method

In order to investigate the behaviour of the suspended fibres, the fibres are visualised with a CCD-camera, which captures images from underneath the flow. Image analysis is used to find the orientation and the velocity of the fibres. Furthermore the velocity profile of the fibres is measured and found to coincide well with the theoretical velocity profile defined in equation 5, which

makes it possible to determine the distance from the wall of individual fibres based on their velocity.

2.4a. *Visualisation.* The CCD-camera (SONY DFW-X700, 1024x768 pixels) visualising the fibres was mounted underneath the flow at  $x = 750$  mm (camera position P4 in figure 5) in order to capture images for orientation studies. To find the velocity profile of the fibres the camera was also mounted at the side of the flow, camera position P1–P3 in figure 5. A stroboscope (Drelloscop 200) was synchronised to the CCD-camera in order to illuminate the field of view. A typical image captured by the camera is shown in figure 6.

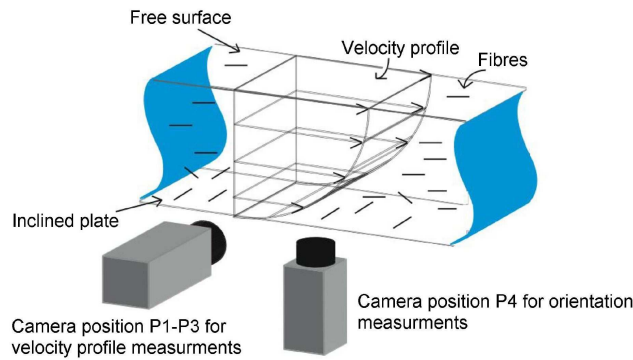


FIGURE 5. Schematic figure illustrating the flow situation with the camera positions P1-P3 and P4.

2.4b. *Image analysis.* To find the position and orientation of the individual fibres in the captured images a 2<sup>nd</sup> order ridge detector is used Jacob & Unser (2004). The correlation between a captured image and the filter in figure 7, is calculated. A high value of the correlation at a certain position in an image indicates that there is a local similarity of the fibre and the filter at that position. The filter is within the class of steerable filters, which means that the correlation of the filter, rotated to a certain angle, with the image can be found through a linear combination of a limited amount of correlations of filters with the image. Thus, it is not necessary to perform correlations for a large number of rotated versions of the filter with the image. For the particular filter used, only three correlations are performed in order to find the angle of the filter that will result in the highest correlation of the filter for each position in the image.

2.4c. *Particle tracking velocimetry.* To find the velocity of the fibres at a certain time, three consecutive images were captured with a frequency of  $f = 10.27 \pm 0.05$  Hz. Between every set of three images a delay of  $T_s = 12$  s was

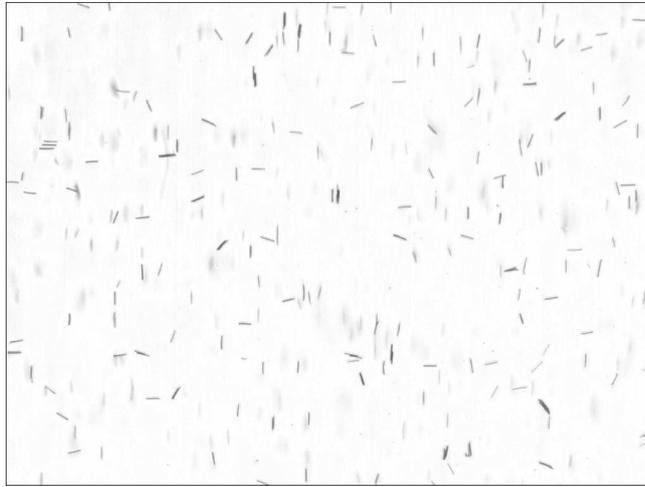


FIGURE 6. Image captured underneath of the flow for orientation studies (camera position P4).

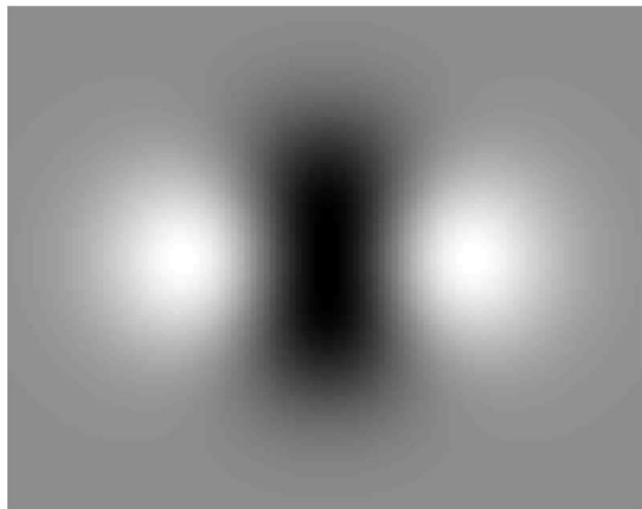


FIGURE 7. Filter used to find the orientation of the fibres.

implemented. This will give the majority of the fibres an opportunity to pass the field of view, which that the following triplet of images will be statistically independent. This aspect will be returned to below. Each measuring series lasted for approximately one hour, resulting in 900 images to analyse.

Based on the position of the fibres in the images the velocity can be found through a Particle Tracking Velocimetry (PTV) algorithm that locates the individual fibres in subsequent images. The principal idea of the algorithm is to start from the position of a fibre in an image and search for fibres in the flow direction in a narrow region downstream of this position in the following (second) image. The velocity is calculated for all the candidate fibres found in the prescribed region of the second image.

Based on the calculated velocities, the positions in the narrow region in the third image, where the fibres would be located if they continued with the same velocity, are calculated. If a fibre is located at any of the proposed positions in the third image it is considered to be the same fibre as the original fibre in the first image. This method is not flawless since it is possible for three different fibres, all travelling with different velocities, to result in a match in the algorithm. Analysing longer image sequences could reduce this problem. This would however decrease the maximum velocity that can be detected. Decreasing the width of the region where the fibres have to be found in the second image, as well as decreasing the area where the fibre has to be found in the third image, can also reduce the error. In the studies performed here, only three images have been used to track the fibres and incorrect matches do appear occasionally, as will be seen in the velocity profile measurements.

2.4d. *Permissible regions for PTV.* In order to ensure statistically independent samples of the orientation and velocity of fibres, it is necessary that each fibre is sampled only once. This is achieved by limiting the region where the fibres have to be found in the first image. The permissible region is shown in figure 8 where a typical image is shown in (a) and the region where fibres have to be found for different velocities is shown in (b). This region is defined so that (i) detection in two subsequent sets of three images is avoided (for low velocities) and (ii) the fibre is still located in the field of view when the third image is captured. In order for a fibre to be detected it has to be located below the solid line. For fibres travelling at velocities lower than  $\Delta X/T_s$ , where  $\Delta X$  is the physical length of the image in the flow direction, the slope of the solid line is defined by the period  $T_s$ . Fibres located in this region travel too slow to pass the field of view in the period  $T_s$ . Thus, if a fibre is located above the solid line, it should have been found in the preceding set of three images. Hence, fibres with velocities smaller than  $\Delta X/T_s$ , located above the solid line, are not considered.

The second effect that has to be taken into account is that the region where a fibre can be detected decreases with an increased velocity of the fibres. The largest detectable velocity of a fibre is  $\Delta X f/2$ . For a fibre travelling with this velocity to be detected it has to be located sufficiently far upstream in the first image, so that it can be found in the two subsequent images. For fibres travelling at velocities larger than  $\Delta X/T_s$ , the slope of the solid line in figure

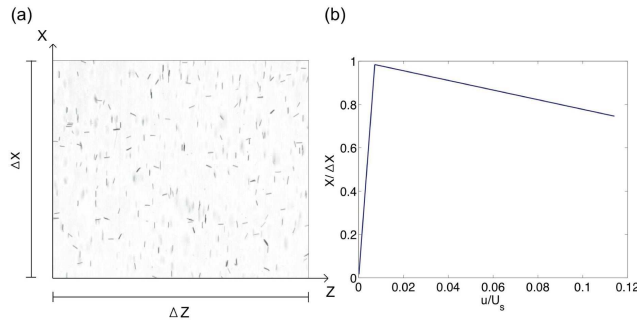


FIGURE 8. Region in image where fibres can be detected.

8(b) is thus defined by the period  $2/f$ . Fibres located above the solid line in the first image will leave the field of view, before the third image is captured. This effect is also present at velocities smaller than  $\Delta X/T_s$ , although since  $2/f \ll T_s$ , the slope of the solid line does not change substantially.

### 2.5. Velocity profile of fibres

To verify that there was no acceleration in the flow and that the velocity profile was fully developed, the camera was mounted at the side of the flow, camera positions P1-P3 ( $x = 650, 750$  and  $850$  mm), see figure 4 and 5. The measurements in this configuration were performed on the smooth surface at an early stage of this work in order to validate the setup and therefore, the fibre suspension was not identical to the suspension used for the orientation studies. The length and diameter of the fibres was  $l = 2$  mm and  $d = 50$   $\mu\text{m}$  respectively and the concentration of fibres was  $nl^3 = 0.31$ . The liquid mixture was essentially the same as mentioned earlier. The results from these measurements are shown in figure 9, where the velocities of individual fibres are marked with dots. The solid line in the figure is the theoretical velocity profile, defined by equation 5. The velocity has been normalised with the surface velocity of the liquid film  $U_s$  and the distance from the wall is normalised with the film thickness  $h$ . The velocities of most of the fibres found coincide very well with the theoretical profile. However, a few of the dots deviate substantially from the theoretical profile, although the amount of these dots is very small compared to the amount of fibres coinciding with the profile. It is believed that the deviating dots are a result of incorrect matches in the particle-tracking algorithm. If the deviating dots are disregarded it can be concluded that there is a strong correlation between the velocity and the distance from the wall of the fibres. This makes it possible to convert the determined velocity of the fibres to a distance from the wall.

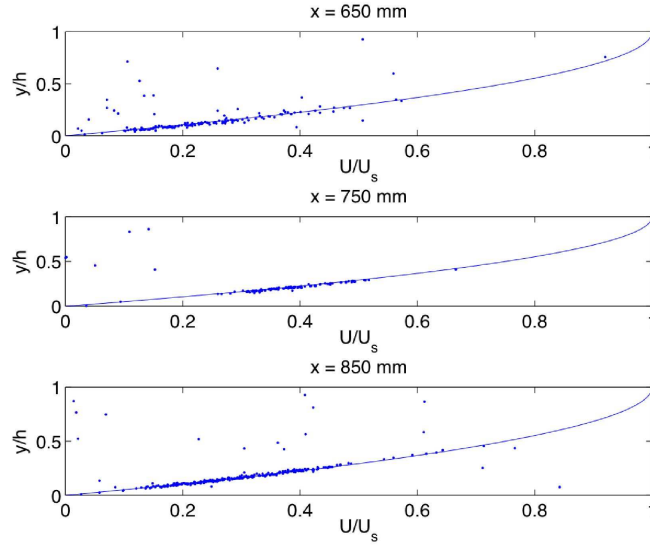


FIGURE 9. Velocity profiles measured at three different position along the x-axis (camera position P1-P3).

### 3. Relevance for paper manufacturing

In a paper machine, the jet leaving the headbox can reach velocities of more than 30 m/s. A natural question that arises is whether the fibre dynamics in the present experiments has any relevance for the fibres flowing over the lamellas in a headbox. The experiments are performed at a 400 times higher viscosity and 1/200 of the velocity as compared to the situation in the headbox. This issue will be discussed in terms of boundary layers and the forces exerted on a fibre in the headbox flow and turbulent/laminar retransition.

#### 3.1. *Fibres close to the headbox walls*

Below, rough estimations of the force distribution exerted on a fibre in the headbox boundary layer and in the present experiments will be compared. An estimation of the velocity profiles along the lamellas in the headbox is given by the similarity solution for flow in a two-dimensional convergent channel, see Schlichting (1979). The velocity  $u$  is given by

$$\frac{u}{U_e} = 3 \tanh^2 \left( \frac{\eta}{\sqrt{2}} + 1.146 \right) - 2, \quad (9)$$

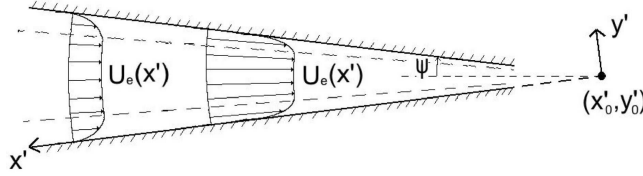


FIGURE 10. Two-dimensional convergent channel.

where  $U_e$  is the velocity of the fluid outside the boundary layer and  $\eta$  is defined as

$$\eta = y' \sqrt{\frac{U_e}{-(x' - x'_0)\nu}}. \quad (10)$$

The definitions of the coordinates  $x'$  and  $y'$  are shown in figure 10.

$U_e$  will grow as the fluid travels downstream due to the contraction. The acceleration will also force the boundary layer thickness to decrease in the downstream direction. Lamellas implemented in a headbox typically ends about 100 mm upstream from the outlet of the headbox. At this position the boundary layer thickness will be of the order of 1 mm. At a distance from the solid surface of 0.5 mm, *i.e.* one fibre length, the shear rate is about  $1000 \text{ s}^{-1}$ . For comparison, the shear rate at the same distance from the surface in the experiments is about  $20 \text{ s}^{-1}$ .

The force on the fibres is estimated under the assumption that they are standing still, straight up from the wall. This assumption is very rough and the following analysis should only be seen as an order of magnitude analysis. If one wants to compare the motions of free fibres, careful analysis at the correct particle Reynolds numbers has to be performed. Attempts in this direction are reported in the literature, and show that fairly small Reynolds number can have a substantial effect on the fibre motion, Subramanian & Koch (2005), but the complete description is yet to be established.

The force on a fibre standing straight up is estimated as follows. The velocity of the fluid surrounding the fibre is assumed to be linear with a shear rate  $\dot{\gamma}$  and thus forms a linear velocity field  $U = (a + 0.5)\dot{\gamma}$  along the fibre. The coordinate  $a$  has its origin in the centre of mass of the fibre and is directed along the fibre with value -0.5 and 0.5 at the fibre centre points, respectively.

This velocity field gives rise to a force distribution on the fibre which can be estimated by integrating the local force per unit length on the fibre from one end to the other. In the experimental configuration the maximum  $Re_d$  is 0.001. For  $Re_d = Ud/\nu$  up to approximately 1, the force is given by White

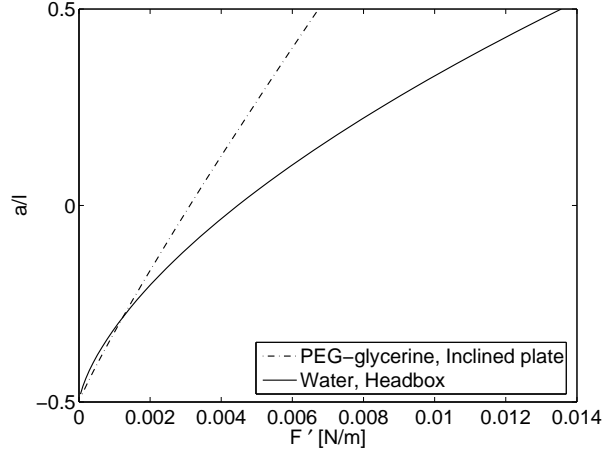


FIGURE 11. Estimated force distribution along fibres standing straight up from the wall in the experiments (— · —) and in a headbox (—) .

(1991)

$$F' = \frac{\rho U^2}{2} \frac{8\pi d}{\text{Re}_d(0.5 - \Gamma + \ln(8/\text{Re}_d))}, \quad (11)$$

where  $F'$  is the force per unit length and  $\Gamma = 0.57722\dots$  is the Euler-Mascheroni constant. In the headbox the largest  $\text{Re}_d$  is about 25 and the force distribution is estimated by

$$F' = \frac{\rho U^2}{2} d C_d \quad (12)$$

where  $C_d$  is given by  $C_d = 1 + 10.0/(\text{Re}_d^{2/3})$ , a correlation valid up to  $\text{Re}_d \approx 250000$ , see White.

The particle Reynolds numbers,  $\dot{\gamma}l^2/\nu$ , are typically 0.01 and 250 in the present experiments and a paper machine, respectively. Thus, inertial effects are considerable in the industrial application and the fibres cannot be expected to perform Jeffery orbits. Nevertheless, it will be shown below that the forces acting on a steady fibre can be expected to be of the same order.

By using equations 11 and 12 and letting  $\text{Re}_d$  and  $U$  vary along the fibre, the force per unit length along the fibre can be calculated. The resulting force distribution for the present setup and in a paper machine is presented in figure 11. The lines are based on a velocity of the outgoing jet of 15 m/s, jet height of 10 mm and a half contraction angle  $\psi = 7^\circ$  (see figure 10). In spite of the large differences in the shear rate and the viscosity between the performed

experiments and the situation in the headbox, the force that the fibres will be subjected to, based on the assumption that the fibre is held fixed in the gradient direction, will only differ by a factor less than 2.5.

### 3.2. Turbulence in headbox

The flow in a headbox is normally considered to be turbulent. However, a turbulent boundary layer can return to laminar-like conditions if it is subjected to a strong acceleration. The acceleration is usually measured by the non-dimensional acceleration parameter

$$K = \frac{2\nu \tan \psi}{q}, \quad (13)$$

where  $q$  is the total flow rate per unit width in the convergent channel. Experiments performed on a turbulent boundary layer for various rates of the free-stream acceleration show that an apparent re-transition to a laminar boundary layer was found by Moretti & Kays (1965) for  $K > 3.5 \cdot 10^{-6}$ . Another experimental study, by Parsheh (2001), of a flat-plate fully turbulent boundary layer subjected to an acceleration in a two-dimensional contraction showed that at  $K \approx 3.1 \cdot 10^{-6}$ , the velocity profile approached a self-similar laminar state at the end of the contraction. As seen in equation 13  $K$  will depend on the flow rate in the headbox as well as the contraction ratio, defined by the angle  $\psi$ . In a papermachine,  $K$  is typically between  $5 \cdot 10^{-7}$  and  $6 \cdot 10^{-6}$ . It is thus possible that the boundary layers will be re-laminarised towards the end of the nozzle for some configurations. To the authors knowledge, all studies performed concerning the re-laminarisation of boundary layers are performed on one-phase flows, *i.e.* no particles have been suspended in the fluid.

## 4. Results & Discussion

Close to a solid surface it is not possible for fibres to perform all the Jeffery orbits illustrated in figure 2, since they would hit the wall when doing so if they are too close to the solid surface. For the case of  $\beta = 0$  ( $C \rightarrow \infty$ ), *i.e.* fibres aligned with the flow, it has been shown that fibres can interact irreversibly with the wall and "pole-vault" up to a position where the Jeffery orbit is possible to perform, Stover & Cohen (1990).

In the following, the restraint given by the Jeffery orbit will be examined further. This will be followed up with experimental data of the orientation of fibres in the  $xz$ -plane. In addition to the orientation of the fibres, their velocities are determined. The velocity of the fibres, together with the known velocity profile, can then be used to determine the distance from the wall to the fibre. A strong effect on the orientation is found for the smooth surface but not for the one with ridges. The coordinate system used in the presentation of the results is defined in figure 2 and 4.

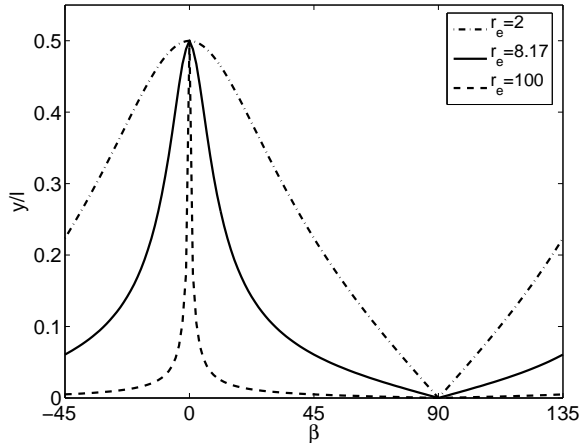


FIGURE 12. Minimum distance from the wall where fibres performing Jeffery orbits can occur for different orientations and aspect ratios of the fibres.

#### 4.1. Jeffery orbits close to the wall

For distances more than one fibre length away from the wall small effects of the presence of the wall have been seen. In this region most of the fibres keep their initial orientation, *i.e.* aligned with the flow. It was observed that fibres spend most of their time aligned with the flow and occasionally flip 180 degrees around the vorticity axis. Although no measurements have been carried out in order to determine the periodicity of the motion, it appears as the fibres perform a motion similar to Jeffery orbits with a high value of  $C$ , as shown in figure 2. When  $C \rightarrow \infty$  the amplitude of the orbit, in the  $y$ -direction is  $l/2$ . For distances from the wall closer than  $l/2$  it is not possible for the fibres to perform this orbit without hitting the wall. As the distance to the wall decreases, the set of possible Jeffery orbits a fibre could perform is reduced. The only orbit that would be possible at the wall is the orbit the given by  $C = 0$ . The possible values of  $\beta$  for fibres performing Jeffery orbits in the near wall region are shown in figure 12. It is not possible for a fibre to perform a Jeffery orbit without hitting the wall if its combination of orientation and distance from the wall lies within the region below the solid line. It should be emphasised that this is only the case if the fibres are actually performing Jeffery orbits. As mentioned before, this assumption is reasonable for fibres close to the wall Pozrikidis (2005) and also at semi-dilute concentrations Koch & Shaqfeh (1990).

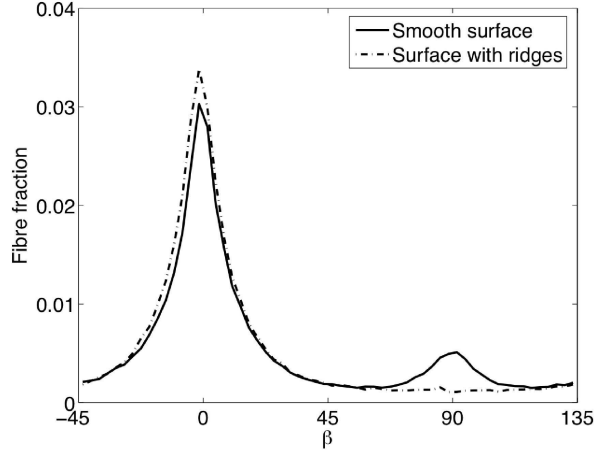


FIGURE 13. Angular distribution of fibres before particle-tracking analysis (camera position P4).

If a fibre would be located in the region below the line, the motion of the fibre could not possibly be described by equations (1 - 4).

#### 4.2. Fibre orientation

4.2a. *Angular distribution prior to particle-tracking analysis.* In figure 13, the normalised distributions of orientations found in the images are shown. Data is shown for fibres flowing over the smooth (solid) and structured (dash-dot) surface. The distributions are determined based on 99760 fibres detected over the smooth surface and 100483 over the ridges. Since these values differ less than one percent, it is reasonable to conclude that the fibre orientation detection algorithm described above works as it should also in the case with the structured surface. The two distributions in figure 13 are fairly similar where the main part of the fibres appear at  $\beta = 0$ , *i.e.* aligned with the flow. There is however one major difference, over the smooth surface, there is a considerable amount of fibres aligned *across* the flow direction, at  $\beta = 90^\circ$ , which can be seen as a bump in the distribution function.

The data presented in figure 13 is based on images captured with the focus of the camera set at  $y = 0$ , *i.e.* at the wall. The depth of focus, measured as the region where almost all fibres are detected by the algorithm, was approximately 1 mm. Thus, the distribution functions in figure 13 are integrated over this region.

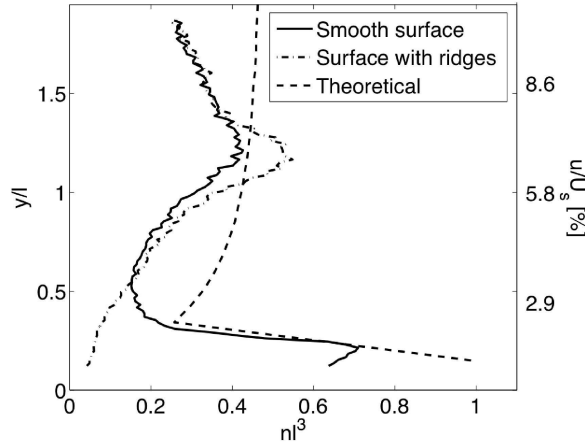


FIGURE 14. Variations in concentration as a function of the distance from the wall (camera position P4).

4.2b. *Wall-normal concentration distribution.* In order to obtain a more detailed knowledge of the how the wall influences the fibre orientation, the velocity of individual fibres, given by the particle tracking algorithm, will be used. For the smooth surface, the known velocity profile gives a one-to-one relation between the velocity and distance to the wall of a fibre (assuming that the fibres follow the flow). Over the structured surface, this relation is less straightforward due to the complex and three-dimensional flow field that will appear close to the surface. This is reflected in the number of fibres which fulfils the conditions for having the velocity determined, as described previously. Over the smooth surface, the velocity of 12164 fibres is determined whereas only 10530 remain after the particle tracking algorithm for the case over the structured surface. When comparing these numbers with the 100 000 fibres found in total, it has to be remembered that three consecutive images are used to determine one velocity value and that some parts of the images are not used in order to ensure statistically independent samples. Nevertheless, a considerable amount of fibres seem to be lost over the structured surface. Therefore, the results below have to be interpreted with care for this case.

Based on the velocities and the known velocity profile (equation 5), concentration profiles can be determined. Such profiles are shown in figure 14 for the two cases (solid and dash-dot as in previous graph) together with a profile calculated based on the (very low but still significant) sedimentation velocities of the fibres (dash). The data will be discussed below, but first the origin of the theoretical curve has to be explained.

The theoretical line is calculated based on three assumptions, (i) that the fibres are evenly distributed at the inlet of the test section ( $x = 0$ ), (ii) that the streamwise velocity of the fibres is given by the local flow velocity given by equation (5) and the wall-normal velocity by the sedimentation speed of a fibre oriented normal to gravity (this assumption is valid since the inclination of the plate is quite small and the fibres spend most of the time with this orientation to gravity) and (iii) that fibres stay very close to the wall once they have fallen down to this region.

This simplified analysis, which neither includes the wall effect on the sedimentation speed nor other aspects of the situation, is only used in order to get a qualitative understanding of the phenomena.

The sedimentation velocity is calculated based on the sedimentation velocity of the fibres, which is given as

$$v_s = \frac{(\rho_p - \rho_f)d^2}{16\nu\rho_f} \left( \ln(2r) + 0.193 + O(\ln(2r)^{-1}) \right) g, \quad (14)$$

where  $r$  is the aspect ratio of the fibres and  $g$  is the acceleration due to gravity, see Herzhaft & Guazzelli (1999) and Batchelor (1970). The assumptions above make it possible to calculate an expected concentration variation at  $x = 750$  mm, where the measurements are taken. It is seen that the assumptions above give a concentration (measured by  $nl^3$ ) that decays from 0.48 to around 0.25 closer to the wall. In the region closest to the wall, there is a sharp peak due to the fact that the fibres are assembled at the wall. The reason why the concentration decays towards the wall at first is that the streamwise velocity decreases towards the wall, and thus the angle at which the fibres are transported becomes steeper and steeper.

The experimental data from the flow over the smooth surface in figure 14 (solid) show a somewhat different behaviour even though the qualitative profile is similar to the theoretical up to  $y/l \approx 1.25$ , a high concentration close to the wall (*i.e.* a lot of slow fibres), followed by a decrease and then an increase up to  $nl^3 \approx 0.4$  at  $y/l = 1.25$ . Above  $y/l = 1.25$ , the number of fibres found in the images decreases due to the limited depth of focus of the camera.

For the flow over the structured surface, the concentration profile in figure 14 looks completely different and does not have the sharp peak close to the wall and the overshoot at  $y/l \approx 1.25$  is considerably stronger. These differences have to be interpreted in the light of the complex flow field over the structured surface. For a complete understanding, the flow over the ridges would have to be studied in detail, but it can be assumed that the ridges induce wall normal movements and (at least locally over the ditches) higher velocities close to the wall. These features of the liquid flow could explain the smaller amount of slow fibres.

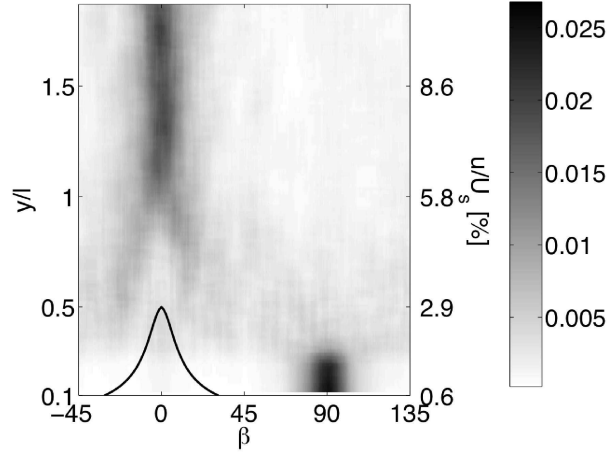


FIGURE 15. Fibre fraction as a function of  $\beta$  for different distances from the wall. Measurements performed on smooth surface (camera position P4).

As will be seen below, the sharp peak in the concentration profile close to the wall (or at small velocities) over the smooth surface in figure 14 is related to the bump in the orientation distribution at  $\beta = 90^\circ$  in figure 13.

The fact that a large number of fibres are present very close to the wall is in conflict with the mechanism of "pole-vaulting" previously proposed Stover & Cohen (1990). This discrepancy will be elaborated further on.

4.2c. *Orientation at various distances from the wall.* Finally, it is possible to look at the distribution at various distances (*i.e.* for fibres of different velocities) from the wall. These results are shown in figure 15 (smooth surface) and 16 (surface with ridges). In these figures, the orientation distributions for each distance from the wall are normalised in order to compensate for the varying concentration. The line defining the region in which Jeffery orbits can be performed (see figure 12) is shown as a solid line.

Starting with the smooth surface, it is seen that almost all of the fibres that have collected at the wall are oriented normal to the flow direction. Thus, the bump in the orientation distribution in figure 13 originates from fibres positioned close to the wall.

This is somewhat surprising, since there are a lot of orientations which are allowed according to the Jeffery orbit. A possible explanation for this could be that close to the surface, where the velocity is very low, the fibres have performed a large number of orbits. Since the period is 2–3 s, the distance 750 mm and the velocity  $< 3$  mm/s, the number of orbits performed are in

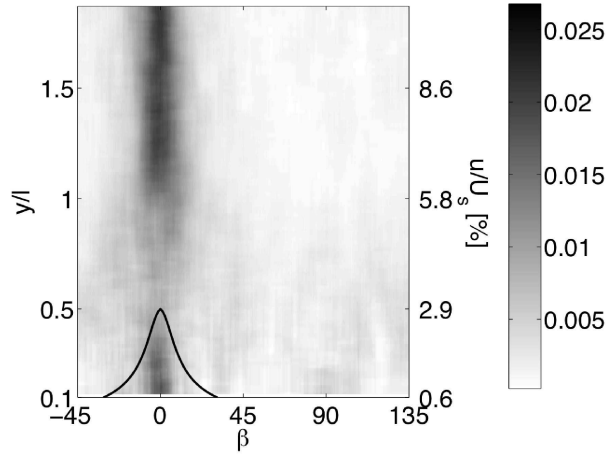


FIGURE 16. Fibre fraction as a function of  $\beta$  for different distances from the wall. Measurements performed on surface with ridges (camera position P4).

the order of 100. It is thus possible that instead of performing the pole-vault previously observed by Stover & Cohen, the fibres are interacting with the wall through lubrication or direct contact and transfer to orbits with lower and lower  $C$  values (see figure 2) for each period. Finally,  $C$  would be close to 0 and the orientation is consequently close to  $\beta = 90^\circ$ . The fact that this, or any other mechanism that leads to  $\beta = 90^\circ$  occurs, implies that the previously observed mechanism for wall interaction is not the only possible one.

Further out from the wall, the fibres illustrated in figure 15 seem to be more evenly distributed over the orientations from  $y/l = 0.2$ –1 and concentrated around  $\beta = 0$  further out.

It is now time to take a closer look at the data from the flow over the structured surface. Before doing so, it is appropriate to remind the reader that the correlation between fibre velocity and distance from the wall is not valid in this case. It is therefore more appropriate to talk about fast and slow fibres. The orientation distribution for different fibre velocities is shown in figure 16 (the corresponding distance from the wall over the smooth surface is also shown). For fibres with a velocity down to that corresponding to  $y > 0.2l$ , the data is very similar to the smooth surface case. For  $y > l$ , most fibres are oriented in the flow direction, in the region  $0.2l < y < l$  the distribution of fibre orientations is more homogeneous. The (very few, compare figure 14) slow fibres are oriented in the streamwise direction.

There are two possible reasons why there is only a small amount of fibres with low velocities detected over the structured surface. The first is that the detection algorithm (which relies on that the fibres move straight downstream) fails. The second is that there are fewer slow fibres. These two effects are probably combined. During the experiments it was observed that fibres were trapped in the ridges and followed the ridges for a while before continuing downstream. As mentioned above, the complex flowfield over the surfaces with ridges, with transversal, wall-normal and streamwise velocity fluctuations might also allow the fibres to travel faster, even though they are closer to the surface. Nevertheless, figure 13 clearly shows that there is no large portion of fibres with  $\beta \approx 90^\circ$  over the structured surface even before the particle tracking algorithm. It has thus been shown that the smooth surface gives the fibres collecting at the wall an orientation  $\beta = 90^\circ$  and that this effect is not present over the surface with ridges.

## 5. Conclusions

An experimental study has been performed on the subject of how fibres orient themselves in a shear flow close to a solid wall. A fibre suspension was allowed to flow down an inclined plate, thus forming a well-defined shear layer. As a visualisation tool a CCD-camera was mounted underneath the flow in order to find the orientation of the fibres in the plane parallel to the wall. Experiments were performed with two different surface structures of the plate to explore the possibility of influencing the orientation of the fibres by modifying the structure of the wall. The first structure used was a plain smooth surface, while the other surface used was a surface with ridges oriented -30 degrees to the direction of the flow. For distances from the wall larger than one fibre length basically all fibres stayed aligned with the flow, for both surfaces. The fibres located in this region seemed to perform orbits similar to those described by Jeffery's mathematical analysis. For distances from the wall closer than one fibre length a difference could be seen between the experiments performed on different surfaces.

For the smooth surface the majority of the fibres no longer oriented themselves in the flow direction. Very close to the wall, less than about a quarter of a fibre length, nearly all of the fibres were oriented close to perpendicular to the flow direction.

Concerning the experiments performed on the surface with ridges, it is concluded that the particle-tracking algorithm used to follow the fibres, fails to do this in a satisfactory manner. The reason for this is probably the disordered motion occurring close to the structured surface, where some of the fibres change direction as they flow down the plate. It is thus not perfectly clear what happens close to the surface with ridges. Nevertheless, it has been possible to show that the effect found close to the smooth surface, where many fibres

orient themselves perpendicular to the flow, is not present for the structured surface with ridges.

The insights of the present study gives two main directions for future work, the first is to study the selection between the "pole-vault" mechanism of fibres close to the wall identified earlier by Stover & Cohen and other mechanisms, leading to  $\beta = 90^\circ$ . The second direction, which is critical for industrial applicability, is to study the orientation at higher velocities/lower viscosities in order to study the effects of inertia and turbulence.

### **Acknowledgments**

Thanks go to Dr. Richard Holm for performing initial experiments and providing valuable input in the startup of the project. Dr. Söderberg has been funded through the Biofibre Materials Centre (BiMaC) at KTH, Mr. Carlsson and Dr. Lundell has been funded by the European Commission under contract number 500345 (NMP2-CT-2004-500345). Dr. Lundell has also been funded by the Swedish Research Council (VR).

## References

- ACHESON, D. J. 1990 *Elementary Fluid Dynamics*. Oxford University Press.
- BATCHELOR, G. 1970 Slender-body theory for particles of arbitrary cross-section in Stokes flow. *J. Fluid Mech.* **44**, 419–440.
- BINDER, R. C. 1939 The motion of cylindrical particles in viscous flow. *J. Appl. Phys.* **10**, 711–713.
- BRETHERTON, F. P. 1962 The motion of rigid particles in a shear flow at low Reynolds number. *J. Fluid Mech.* **14**, 284–304.
- COX, R. G. 1971 The motion of a long slender body in a viscous fluid. Part 2. Shear flow. *J. Fluid Mech.* **45**, 625–657.
- FELLERS, C. & NORMAN, B. 1998 *Pappersteknik*. KTH, Stockholm, Sweden.
- HERZHAFT, B. & GUAZZELLI, E. 1999 Experimental study of the sedimentation of dilute and semi-dilute suspensions of fibres. *J. Fluid Mech.* **384**, 133–158.
- HOLM, R. 2005 Fluid mechanics of fibre suspensions related to papermaking. PhD thesis, Royal Institute of Technology, Stockholm, Sweden.
- ISO, Y., KOCH, D. L. & COHEN, C. 1995 Orientation in simple shear flow of semi-dilute fiber suspensions. 1. Weakly elastic fluids. *J. Non-Newtonian Fluid Mech.* **62**, 115–134.
- JACOB, M. & UNSER, M. 2004 Design of steerable filters for feature detection using Canny-like criteria. *IEEE T. Pattern Anal.* **26** (8), 1007–1019.
- JEFFERY, G. B. 1922 The motion of ellipsoidal particles immersed in a viscous fluid. *Proc. Roy. Soc. London A* pp. 161–179.
- KOCH, D. L. & SHAQFEH, E. S. G. 1990 The average rotation rate of a fibre in the linear flow of a semidilute suspension. *Phys. Fluids A* **2**, 2093–2102.
- MORETTI, P. M. & KAYS, W. M. 1965 Heat transfer to a turbulent boundary layer with varying free-stream velocity and varying surface temperature - An experimental study. *Int. J. Heat Mass Transfer* **8**, 1187–1202.
- MOSES, K. B., ADVANI, S. G. & REINHARDT, A. 2001 Investigation of fiber motion near solid boundaries in simple shear flow. *Rheol. Acta* **40**, 296–306.
- PARSHEH, M. 2001 Flow in contractions with application to headboxes. PhD thesis, Royal Institute of Technology, Stockholm, Sweden.
- PETRICH, M. P., KOCH, D. L. & COHEN, C. 2000 An experimental determination

- of the stress-microstructure relationship in semi-concentrated fiber suspensions. *J. Non-Newtonian Fluid Mech.* **95**, 101–133.
- POZRIKIDIS, C. 2005 Orbiting motion of a freely suspended spheroid near a plane wall. *J. Fluid Mech.* **541**, 105–114.
- SCHLICHTING, H. 1979 *Boundary layer theory*, 7th edn. McGraw-Hill.
- STOVER, C. A. & COHEN, C. 1990 The motion of rodlike particles in the pressure-driven flow between flat plates. *Rheol Acta* **29**, 192–203.
- SUBRAMANIAN, G. & KOCH, D. L. 2005 Inertial effects on fibre motion in simple shear flow. *J. Fluid Mech.* **535**, 383–414.
- TAYLOR, G. I. 1923 The motion of ellipsoidal particles in a viscous fluid. *Proc. Roy. Soc. London A* **103**, 58–61.
- WHITE, F. M. 1991 *Viscous fluid flow*, 2nd edn. McGraw-Hill.



## Paper 2



# Orientation of fibres in a flowing suspension near a plane wall

By Allan Carlsson<sup>†</sup>, Fredrik Lundell<sup>†</sup> & L. Daniel Söderberg<sup>†,‡</sup>

<sup>†</sup>Linné Flow Centre, KTH Mechanics, SE - 100 44 Stockholm, Sweden

<sup>‡</sup>STFI-Packforsk AB, SE - 114 86 Stockholm, Sweden

To be submitted

The wall effect on the orientation of fibres suspended in a shear flow has been studied experimentally. Experiments were performed on two concentrations for fibres of two different aspect ratios,  $r_p = 10$  and  $r_p = 40$ . For all cases the majority of the fibres were oriented close to the flow direction, as initially aligned, for distances further away from the wall than one fibre length. Closer to the wall than one fibre length a distinction could be seen for fibres of different aspect ratio. Fibres of  $r_p = 10$  adopted a more isotropic orientation distribution as the distance from the wall decreased to half a fibre length. Closer to the wall than about a quarter of a fibre length most of the fibres were oriented close to perpendicular to the flow direction. For fibres of  $r_p = 40$  this change of orientation was not seen and the fibres were oriented close to the flow direction also near the wall. Due to the density difference between the fibres and the surrounding fluid an accumulation of fibres was found in the near wall region. For fibres of  $r_p = 40$  the highest concentration was found above  $y = 0.5l$ , whereas for fibres of  $r_p = 10$  a peak in the concentration was found in the very proximity to the wall.

---

## 1. Introduction

Jeffery (1922) derived the equations of motion for a single spheroid suspended in a simple shear flow, assuming that inertia could be totally neglected. These equations are

$$\dot{\phi} = -\frac{\dot{\gamma}}{r_e^2 + 1} (r_e^2 \sin^2 \phi + \cos^2 \phi) \quad (1)$$

$$\dot{\theta} = \left( \frac{r_e^2 - 1}{r_e^2 + 1} \right) \frac{\dot{\gamma}}{4} \sin 2\phi \sin 2\theta, \quad (2)$$

where  $\phi$  is the angle taken in the flow-gradient plane, from the projection of the principal axis of the particle to the direction of the flow. The angle  $\theta$  is

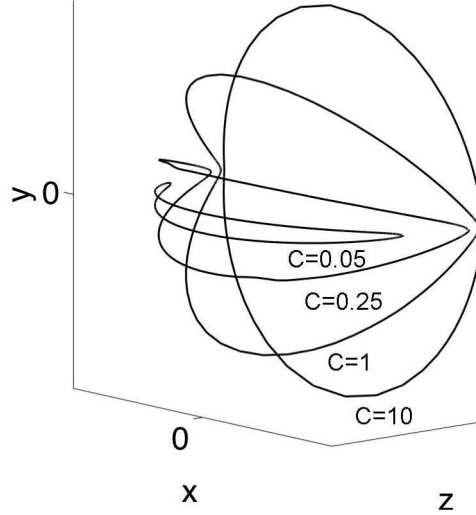


FIGURE 1. The path of a fibre end point for  $r_e = 8$  and different  $C$ -values in Jeffery's equation.

defined as the angle from the vorticity axis to the principal axis of the particle. Furthermore  $\dot{\gamma}$  is the shear rate and  $r_e$  is the spheroidal aspect ratio of the particle, *i.e.* the ratio between the major and minor axis.

Integration of equations (1) and (2) with respect to time yields

$$\tan \phi = \frac{1}{r_e} \tan \left( -\dot{\gamma} t \frac{r_e}{r_e^2 + 1} + \tan^{-1}(r_e \tan \phi_0) \right) \quad (3)$$

$$\tan \theta = \frac{Cr_e}{(r_e^2 \sin^2 \phi + \cos^2 \phi)^{1/2}}, \quad (4)$$

where  $C$  and  $\phi_0$  are constants determined by the initial conditions. In figure 1, where the flow velocity is defined by  $\mathbf{u} = \dot{\gamma} y \mathbf{e}_x$ , Jeffery orbits are shown for different values of  $C$  and  $r_e = 8$ . For  $C = 0$  the principal axis of the spheroid is aligned with the vorticity axis, oriented perpendicular to the flow direction. For high values of  $C$  the particle is oriented in the flow direction most of the time to occasionally, with a constant period, flip 180 degrees around the vorticity axis.

An extension to Jeffery's equations, to be valid also for cylindrical particles, provided that an equivalent aspect ratio of the particle is found, was performed by Bretherton (1962). The orbital motion described by Jeffery was observed experimentally first by Taylor (1923). In Jeffery's derivation there are no fibre-fibre interactions and no wall effects taken into account. The wall effect has

been studied experimentally by Moses, Advani & Reinhardt (2001) and Stover & Cohen (1990). In both studies an agreement with Jeffery's equations was found for distances further away from the wall than one fibre length. In the study by Moses *et al.* only the orbit corresponding to high values of  $C$  was investigated and an increased rate of rotation was found for distances from the wall closer than one fibre length. Stover & Cohen found a longer period than what would be predicted by the shear rate in the near wall region, both for low and high values of  $C$ . Furthermore for fibres with a high value of  $C$ , located closer to the wall than half a fibre length, the fibres interacted irreversibly with the wall. In this region the fibres moved away from the wall to a point where the centre of the fibres was approximately located half a fibre length from the wall. Stover & Cohen referred to this motion as a "pole vaulting" interaction with the wall.

An experiment concerning the relation between the final orientation and aspect ratio of cylindrical particles suspended in a simple shear flow was conducted by Binder (1939). For particles with a cylindrical aspect ratio (length to diameter ratio) less than  $r_p \approx 15$ , an agreement with one of the results of Jeffery's minimum energy hypothesis was achieved. Jeffery proposed that prolate spheroidal particles would tend to adopt the orbit with  $C = 0$ . However for particles of  $r_p > 15$  orbits corresponding to high values of  $C$  was observed, in the experiments performed by Binder (1939).

In the present study experimental measurements on the orientation of fibres, with varying aspect ratios, in planes parallel to a solid surface will be presented. The measurements are purely statistical and no conclusions will be drawn concerning the periodicity of the fibre motion.

## 2. Experimental apparatus & technique

A CCD camera was used in order to visualise flowing fibres, in the proximity of a solid surface. Image analysis made it possible to find the velocity and orientation of the fibres in the plane parallel to the solid surface. Velocity profile measurements verified that the flow was fully developed and revealed a strong correlation between the velocity and the wall normal position of the fibres.

### 2.1. Fibre Suspension

The fibre suspension, used in the experiments, consisted of cellulose acetate fibres suspended in a viscous liquid. The density of the cellulose fibres was  $\rho_p \approx 1300 \text{ kg/m}^3$ . Experiments were conducted on two different aspect ratios,  $r_p = 10$  and  $r_p = 40$ , where the diameter of the fibres was  $d = 50 \text{ }\mu\text{m}$  and the length  $l$  of the fibres was varied. For each aspect ratio of the fibres two different concentrations were used. Expressed as the number of fibres to be found in a volume of  $l^3$  these were  $nl^3 = 0.02$  and  $0.48$  for  $r_p = 10$  and  $nl^3 = 0.48$  and  $3.82$  for  $r_p = 40$ .

| $r_p = l/d$ | $T$ [K]         | $\nu$ [m <sup>2</sup> /s]    | $\rho_f$ [kg/m <sup>3</sup> ] |
|-------------|-----------------|------------------------------|-------------------------------|
| 10          | $295.5 \pm 0.5$ | $(383 \pm 10) \cdot 10^{-6}$ | $1210 \pm 15$                 |
| 40          | $295.5 \pm 0.5$ | $(387 \pm 10) \cdot 10^{-6}$ | $1209 \pm 15$                 |

TABLE 1. Properties of the liquid mixture in which the fibres were suspended.

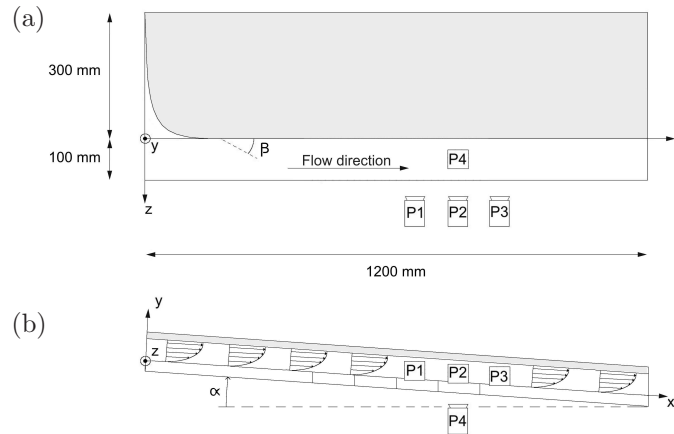


FIGURE 2. Schematic figure of the flow section, (a) Top view, (b) Side view.

The index of refraction of the fibres was approximately matched to that of the liquid. In order to visualise the fibres 100% of the fibres were dyed black for the low concentration cases of  $r_p = 10$  and  $r_p = 40$ . For the cases of higher concentration,  $nl^3 = 0.48$  for  $r_p = 10$  and  $nl^3 = 3.82$  for  $r_p = 40$ , only about 4% and 16% respectively of the fibres were dyed black.

The liquid phase was a mixture of polyethyleneglycol (PEG-400) and glycerine. The properties of the mixture for the two different aspect ratios are summarised in table 1. The density of the liquid is lower than that of the fibres. The fibres will thus sediment slowly when suspended in the liquid.

## 2.2. Velocity field

In the experiments a film of the fibre suspension was flowing down an inclined glass plate. The thickness of the film was  $h = 17.0 \pm 0.2$  mm for the cases when  $r_p = 10$  and  $h = 17.5 \pm 0.2$  mm when  $r_p = 40$ . A schematic figure of the flow section is shown in figure 2. The length of the channel was 1200 mm and the width was defined by an insert, placed on the glass plate. From  $x = 0$  mm to

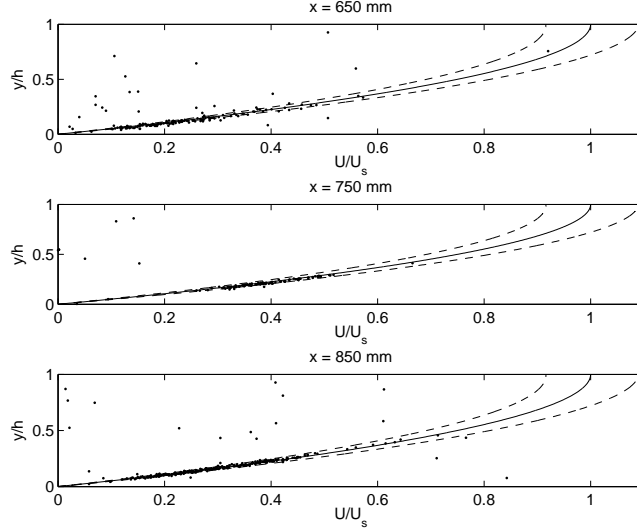


FIGURE 3. Velocity profiles for three different positions in the flow direction,  $x = 650, 750$  &  $850$  mm.

$x = 150$  mm there was a gradual change in the width, from 400 mm to 100 mm. For  $x > 150$  mm the width was constant and equal to 100 mm.

The velocity  $u$  of a film of a Newtonian fluid flowing down an inclined plane is given by

$$u = \frac{g}{2\nu}y(2h - y) \sin \alpha, \quad (5)$$

where  $g$  is the constant acceleration of gravity,  $\nu$  is the kinematic viscosity of the fluid and  $y$  is the wall normal position, where  $y = 0$  at the wall and  $y = h$  at the free surface of the film. Furthermore  $\alpha$  is the angle of inclination of the plane with respect to horizontal. In the present experiments  $\alpha = 2.60 \pm 0.1$ .

To capture the velocity profile of the fibres in the experiments and to make sure that the flow was fully developed, with no acceleration, a CCD camera was mounted on the side of the flow at  $x = 650, 750$  &  $850$  mm (position P1, P2 & P3 in figure 2). In figure 3 the velocity profile is shown. The solid line corresponds to the analytical expression given by equation (5) and the dashed lines are error estimations, of the solid line, based on the accuracy of the measured parameters in equation (5). The dots in figure 3 correspond to velocities of fibres that have passed the field of view during the measurements. The velocity has been normalised with the free surface velocity  $U_s = u|_{y=h}$  and the wall normal position has been normalised with  $h$ . Velocity profile measurements were only made on fibres with  $r_p = 40$  and the concentration for these

specific measurements was  $nl^3 = 0.31$ . By disregarding the few deviating dots, which are due to a mismatch in the particle tracking velocimetry algorithm (see below), it is concluded that the velocity profile is fully developed in the region between  $x = 650$  and  $850$  mm. It is noted that, when the few deviating dots have been disregarded, the velocity of the fibres correlate well with the distance from the solid surface. This fact is used, in the orientation studies, to determine the wall normal distance of the fibres, once the fibre velocities has been computed.

### 2.3. Measurement & Analysis Procedure

For the orientation studies the CCD camera was mounted underneath the glass plate at  $x = 750$  mm (position P4 in figure 2). Images were captured, three at a time, with a frequency of  $f = 10.25 \pm 0.05$  Hz when  $r_p = 10$  and  $f = 10.27 \pm 0.05$  Hz when  $r_p = 40$ . In between every set of three images there was a delay of  $T_s \approx 12$  s. The delay was implemented in order for the fibres to pass out of the field of view before the next set of three images was captured. Therefore the exact length of  $T_s$  is not crucial. The field of view of the images was  $X * Z = 15 * 20$  mm<sup>2</sup> for  $r_p = 10$  and  $X * Z = 12 * 17$  mm<sup>2</sup> for  $r_p = 40$ , where  $X$  is the length of the field of view in the direction of the flow, *i.e.* along the  $x$ -axis, and  $Z$  is the length in the direction of the vorticity, *i.e.* along the  $z$ -axis.

The angle  $\beta$  is defined as the angle in the  $xz$ -plane taken either clockwise or counterclockwise from the flow direction. To determine the orientation  $\beta$  of the fibres a 2<sup>nd</sup> order ridge detector within the class of steerable filters was used, see Jacob & Unser (2004).

In order to find the velocity of the fibres a particle tracking velocimetry algorithm (PTV) was used. The PTV uses information concerning the location of the fibres in three subsequent images. Based on this information the velocity of individual fibres is computed. Fibres found in a set of three images, with a velocity higher than  $X/T_s$ , will leave the field of view before the subsequent set of images are captured, independently on their location in the images. The velocity  $X/T_s$  corresponds to a distance from the wall of  $y \approx d$ . To ensure statistically independent data the  $x$ -position where the fibres has to be found in the images is set to be a function of the fibre velocity  $u_{fib}$ . If  $X_0$  is the  $x$ -position furthest upstream in the images, the fibre has to be found in the region between  $X_0$  and  $X_0 + u_{fib}T_s$ . In this manner the possibility of finding fibres with a velocity lower than  $X/T_s$ , more than once, is eliminated.

Based on the relation between the velocity and  $y$ -position of the fibres, it is possible to transform the computed velocities to wall normal positions, through equation (5). Once this has been done it is possible to study the orientation of fibres for different distances from the solid surface.

| $r_p = l/d$ | $nl^3$ | Region of $y$  | $N$  |
|-------------|--------|----------------|------|
| 10          | 0.02   | $0 < y < 2l$   | 7435 |
| 10          | 0.48   | $0 < y < 2l$   | 6944 |
| 40          | 0.48   | $0 < y < 3l/2$ | 4827 |
| 40          | 3.82   | $0 < y < 3l/2$ | 6281 |

TABLE 2. The number of detected fibres  $N$  in the different measurements.

To be able to determine the fibre concentration as a function of  $y$  it is essential to know the volume  $V = \Delta X \Delta Y \Delta Z$  in where the fibres are detected. In this volume  $\Delta Z = Z$  and  $\Delta Y$  can be chosen arbitrarily, with the help of equation (5), based on the desired resolution in the  $y$ -direction. The distance  $\Delta X = X - 2u_{fib}/f$  is however a function of the fibre velocity, see Carlsson, Lundell & Söderberg (2006). This is due to the fact that the fibres have to be found in three subsequent images and that the fibres will travel a distance within the period it takes to capture these images. Hence, it is not possible to detect fibres of  $u_{fib} > Xf/2$  since these fibres will have left the field of view before the third of three images is captured, independent on their location in the first image.

### 3. Results & Discussion

The total number of fibres  $N$  for which the velocity and orientation have been determined, in all the cases, is shown in table 2. The regions of  $y$  are also shown in table 2 and vary depending on the aspect ratio of the fibres. In the results presented below the regions are divided into a number of subregions in which the angular distribution is computed. The wall normal concentration distribution is also reported.

#### 3.1. Angular distribution in near wall region

Due to the streamwise acceleration in the contraction, between  $x = 0$  and  $x = 150$  mm, the fibres became essentially aligned in the flow direction ( $\beta = 0$ ). The fibre orientation was measured at  $x = 750$  mm. In figure 4 the distribution function  $F(\beta) = P(B \leq \beta)$ , *i.e.* the probability that a fibre will be oriented between the flow direction and a given angle  $\beta$ , is shown for all cases. The figures illustrate how  $F(\beta)$  varies with the distance from the solid surface. The fibre length  $l$  has been used to normalise the distance from the wall.

In figure 4 (a) and (b), showing the cases where  $r_p = 10$ , it is seen that for distances further away from the wall than one fibre length, the majority of the fibres are still oriented close to the flow direction. No significant difference can be seen between the regions  $l < y < 5l/4$  and  $5l/4 < y < 3l/2$ , indicating that the wall has a close to negligible effect for  $y > l$ . However, as soon as the fibres are located closer to the wall than one fibre length  $F(\beta)$  changes character.

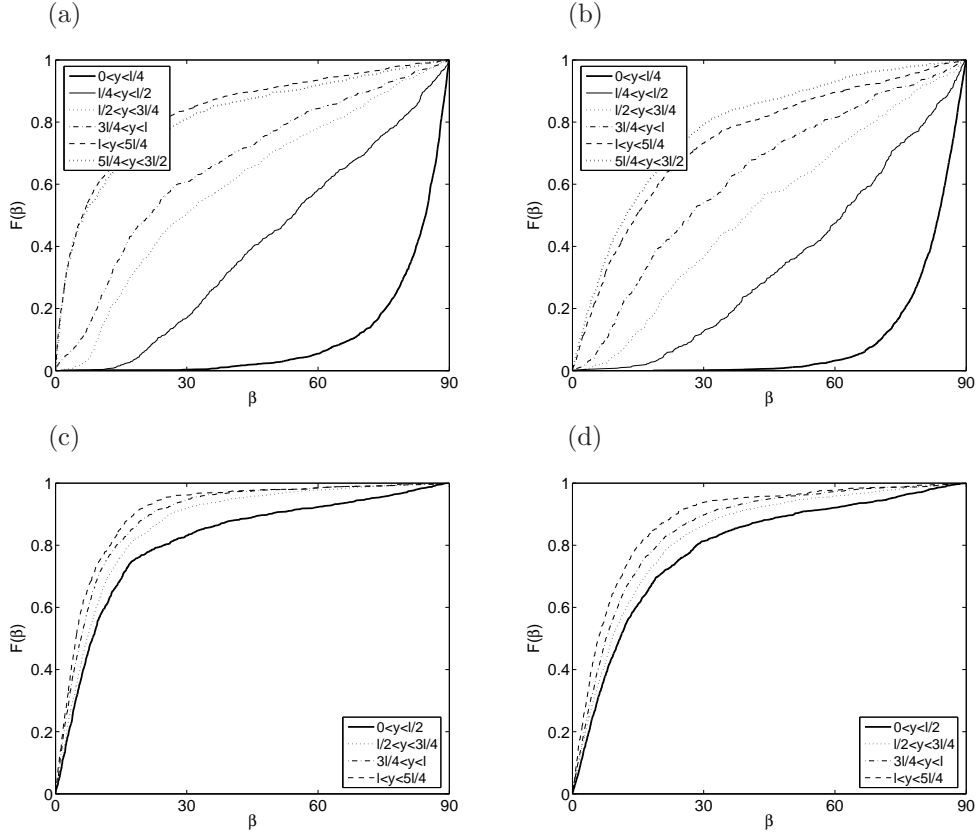


FIGURE 4. Distribution function  $F(\beta)$  for different distances from the wall: (a)  $r_p = 10$  and  $nl^3 = 0.02$ , (b)  $r_p = 10$  and  $nl^3 = 0.48$ , (c)  $r_p = 40$  and  $nl^3 = 0.48$  and (d)  $r_p = 40$  and  $nl^3 = 3.82$ .

A gradual change towards a more isotropic angular distribution occurs as the distance from the wall is decreased to  $y \approx l/2$ . When the distance is decreased even further the fibres tend to orient themselves close to perpendicular to the flow direction ( $\beta = 90$ ) in the region  $0 < y < l/4$ .

The angular distribution at different  $y$ -positions, for fibres of aspect ratio  $r_p = 40$ , are presented in figure 4(c) and (d). In these cases most of the fibres stay oriented close to the flow direction, independent of the distance from the solid surface.

In figure 5  $F(\beta)$  is compared for all cases in two different regions; about one fibre length from the wall,  $\frac{7l}{8} < y < \frac{9l}{8}$ , in (a) and close to the wall,  $0 < y < \frac{l}{4}$

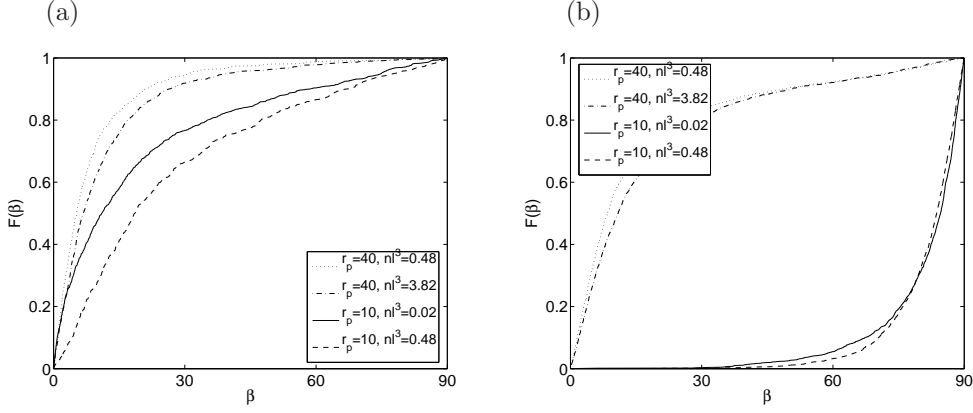


FIGURE 5. Distribution function  $F(\beta)$  for all cases: (a) in the region  $\frac{7l}{8} < y < \frac{9l}{8}$  both for  $r_p = 10$  and 40 and (b) in the region  $0 < y < \frac{l}{4}$  for  $r_p = 10$  and  $0 < y < \frac{l}{2}$  for  $r_p = 40$ .

for  $r_p = 10$  and  $0 < y < \frac{l}{2}$  for  $r_p = 40$ , in (b). The reason for the use of a larger region of study in figure 5(b), for fibres of  $r_p = 40$ , is that the number of detected fibres below  $y = l/4$  is limited and not sufficient to compute  $F(\beta)$ . It is seen, in figure 5(a), that the shape of  $F(\beta)$  is qualitatively the same, for all cases, for  $y \approx l$ . However, an effect is noted: for both aspect ratios  $F(\beta)$  grows faster with  $\beta$ , for small values of  $\beta$ , when the concentration is lower. Also, the probability that fibres are found in  $0 < \beta < 30$  is larger for the longer fibres of  $r_p = 40$  than for the short fibres of  $r_p = 10$ . In the region close to the wall, shown in figure 5(b), it is once more noted that the behaviour of the fibres of different aspect ratios is different. However, the variation in concentration has a small effect on  $F(\beta)$ , in this region.

The reason for the distinction seen between the two different aspect ratios, in the region  $y < l$ , is yet to be explained. A possible explanation could lie in the aspect ratio dependency of the preferred orbital motion, found by Binder (1939). Binder studied the final orientation of cylindrical particles, far from solid walls, in a simple shear flow, for three different shear rates, and found orbits of high  $C$ , see figure 1, for aspect ratios larger than  $r_p \approx 15$  and orbits of  $C = 0$  for smaller aspect ratios. Binder could not explain the observed difference in final orientations, but suggested that the answer might lie in the neglect of inertia in Jeffery's analysis. If the wall functions as a small disturbance, the fibres could tend to adopt their preferential orientation. If this be granted, fibres of  $r_p = 10$  would, according to the results of Binder, transfer to orbits with lower values of  $C$ , while fibres of  $r_p = 40$  would stay at large values of  $C$ .

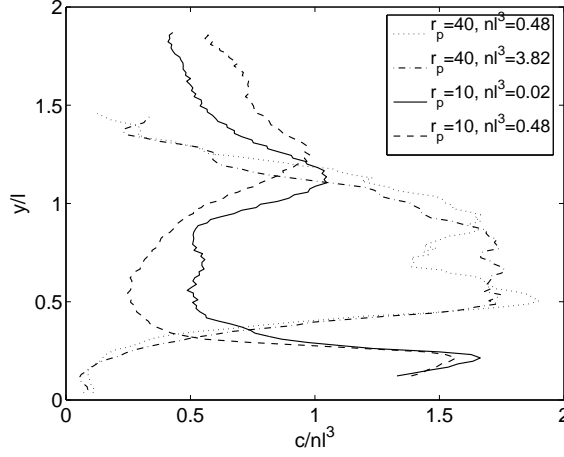


FIGURE 6. Variations in concentration as a function of the distance from the solid surface

### 3.2. Variations in concentration in the wall-normal direction

As mentioned in the previous section the concentrations investigated was  $nl^3 = 0.02$  and  $0.48$  for  $r_p = 10$  and  $nl^3 = 0.48$  and  $3.82$  for  $r_p = 40$ . These are the initial concentrations that one would expect to find if the fibres were homogeneously distributed across the shear layer. In figure 6 the concentration  $c$ , based on the number of fibres found in the detection volume  $V$ , is shown as a function of  $y$ . The concentrations have been normalised with their respective initial concentration. The absolute levels of the concentrations are coupled to threshold values set in the PTV procedure and are uncertain. However the relative distribution of the fibres is approximately the same, independent of the threshold values. This is shown in figure 7 where the threshold values has been modified for two of the cases: (a)  $r_p = 40$  and  $nl^3 = 0.48$  and (b)  $r_p = 10$  and  $nl^3 = 0.02$ . The solid lines correspond to the original threshold values in the PTV, upon which the results presented are based. The other two lines, the dot-dashed and the dashed, correspond to lower and higher threshold values, set in the PTV, respectively. The new threshold values resulted in roughly 10-20% more or less detected fibres as compared to the original threshold values. Since the relative distribution of fibres is unchanged, some conclusions can be drawn concerning the different characteristics seen for  $r_p = 10$  and  $r_p = 40$ .

It is seen in figure 6 that for fibres of  $r_p = 10$  there is a maximum in the concentration very close to the wall. For fibres of  $r_p = 40$  the maximum concentration is found above  $y = l/2$  and few fibres are detected below this level. The density of the fibres is higher than that of the liquid and that is in all probability the reason for the high concentration of fibres in the near wall

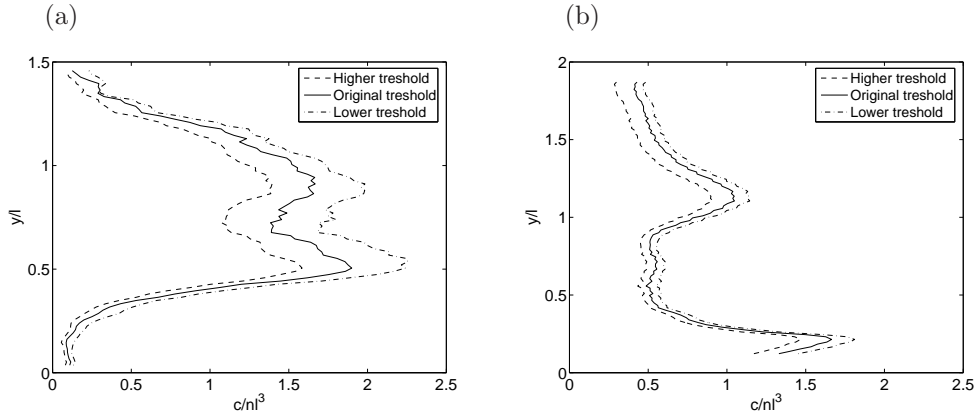


FIGURE 7. Variations in concentration as a function of  $y$  for different threshold values set in the PTV; (a)  $r_p = 40$  and  $nl^3 = 0.48$  and (b)  $r_p = 10$  and  $nl^3 = 0.02$ .

region. A probable reason for the absence of fibres, below  $y = l/2$  for  $r_p = 40$ , is that the fibres perform the "pole vaulting" motion previously found by Stover & Cohen. The "pole vaulting" motion was only observed for high values of  $C$ . For  $r_p = 10$  there are less fibres oriented close to  $\beta = 0$ , see figure 4 (a) and (b), indicating that the fibres tend to adopt lower values of  $C$ , if they are rotating in Jeffery-like orbits, when located closer to the wall than one fibre length. There would thus not be any mechanism that pushes the fibres away from the wall and the fibres would accumulate at the wall.

#### 4. Conclusions

In a fibre suspension flowing down an inclined wall, the fibre orientation was analysed in planes parallel to the wall. Due to a contraction of the flow, located far upstream from the measuring position, the fibres were initially oriented in the direction of the flow. This orientation was found to be the most probable for distances larger than one fibre length from the wall, in all cases investigated. For fibres of  $r_p = 10$  the wall had a large effect on the orientation of the fibres for distances closer to the wall than one fibre length, where a gradual change, from being aligned with the flow at  $y = l$  to being oriented perpendicular to the flow in the very proximity of the wall, was seen. For longer fibres of  $r_p = 40$  the majority of the fibres were oriented close to the flow direction for all distances from the wall.

A difference between fibres of different aspect ratios could also be seen in the wall normal concentration distribution. For fibres of  $r_p = 10$  the maximum concentration was found very close to the wall and for  $r_p = 40$  the maximum

was found at  $y \approx l/2$ . It has been concluded that these high concentrations near the wall are due to the difference in density between the fibres and the fluid. The most probable reason for the different location of the maximums is that fibres of  $r_p = 40$  performs the "pole vaulting" motion reported by Stover & Cohen, while fibres of  $r_p = 10$  do not. The mechanism has only been seen for Jeffery orbits of high  $C$  values, where fibres are oriented in the flow direction and flips around the vorticity axis with regular intervals. For fibres of  $r_p = 10$ , the flow direction is not the dominating orientation in the near wall region. Thus, it is not likely that the fibres would experience the "pole vaulting" motion in this case, resulting in an accumulation of fibres very close to the wall.

## References

- BINDER, R. C. 1939 The motion of cylindrical particles in viscous flow. *J. Appl. Phys.* **10**, 711–713.
- BRETHERTON, F. P. 1962 The motion of rigid particles in a shear flow at low Reynolds number. *J. Fluid Mech.* **14**, 284–304.
- CARLSSON, A., LUNDELL, F. & SÖDERBERG, L. D. 2006 Fibre orientation control related to papermaking. *J. Fluids Eng.*, Accepted for publication.
- JACOB, M. & UNSER, M. 2004 Design of steerable filters for feature detection using Canny-like criteria. *IEEE T. Pattern Anal.* **26** (8), 1007–1019.
- JEFFERY, G. B. 1922 The motion of ellipsoidal particles immersed in a viscous fluid. *Proc. Roy. Soc. London A* pp. 161–179.
- MOSES, K. B., ADVANI, S. G. & REINHARDT, A. 2001 Investigation of fiber motion near solid boundaries in simple shear flow. *Rheol. Acta* **40**, 296–306.
- STOVER, C. A. & COHEN, C. 1990 The motion of rodlike particles in the pressure-driven flow between flat plates. *Rheol. Acta* **29**, 192–203.
- TAYLOR, G. I. 1923 The motion of ellipsoidal particles in a viscous fluid. *Proc. Roy. Soc. London A* **103**, 58–61.



# Paper 3

3



# Evaluation of steerable filters for detection of rod-like particles in flowing suspensions

By Allan Carlsson<sup>†</sup>, Fredrik Lundell<sup>†</sup> & L. Daniel Söderberg<sup>†,‡</sup>

<sup>†</sup>Linné Flow Centre, KTH Mechanics, SE - 100 44 Stockholm, Sweden

<sup>‡</sup>STFI-Packforsk AB, SE - 114 86 Stockholm, Sweden

A filter within the class of steerable filters is evaluated for suitability of finding rod-like particles suspended in flowing suspensions. For small noise levels the steerable filter succeeds in finding artificially generated fibres with well-defined angles. The method is compared to a more computationally expensive method involving convolutions with an oriented elliptic filter. Good agreement is found between the two methods, when analysing a flowing fibre suspension.

---

## 1. Introduction

In order to perform a complete motion analysis of rod-like particles in flowing suspensions it is essential to determine the orientation of the particles, as a function of time. A reliable approach of finding the orientation of particles captured in images is to use oriented filters. This was for instance done by Holm (2005) to find the orientation of fibres in a shear flow. One typically constructs a filter, with a shape resembling the shape of the particles and performs the convolution of the filter with the images. A high value of the convolution at a certain position indicates that the image has a local resemblance with the filter at that position. To find the orientation of the particles the filter has to be rotated to different angles and a convolution has to be performed for each angle. The orientation of a particle is given by the angle at which the convolution results in the highest value. This course of action can however be heavy from a computational perspective since the angular resolution will be proportional to the number of convolutions performed.

From a computational point of view Freeman & Adelson (1991) introduced a more efficient approach, for general feature detection, *i.e.* not restricted to rod-like particles. The term "steerable filters" was introduced in order to describe a class of filters in which a filter of arbitrary orientation can be obtained from a linear combination of a limited amount of "basis filters". In other words it is possible to compute the convolution of the images, containing rod-like particles, with the basis filters and calculate the orientation of the particles

from the responses of the convolutions. In this manner it is possible to cut down on the computational load and still have a good angular resolution.

A method for designing filters, within the class of steerable filters, for 2D feature detection, was proposed by Jacob & Unser (2004). For instance a filter for ridge detection was designed. In the present study this ridge detector is used in order to find the orientation of rod-like particles. The scope of this study is to evaluate how well the method functions in finding the angle of the particles as well as to investigate the sensitivity to noise of the method. This is done by capturing images of a picture containing artificially generated particles with well-defined angles. The paper is finally concluded by a comparison of the method with a more traditional approach, on a case where particles have been suspended in a shear flow.

## 2. Steerable filter for detection of rod-like particles

A rotated version of a steerable filter can be obtained from a linear combination of a limited set of basis filters. Thus, the angle at which the highest response will be found, from the convolution of the steerable filter with the image, at all positions in the image, can be obtained through the convolutions of the basis filters with the image. The class of steerable filters considered in this work can be expressed as

$$h(x, y) = \sum_{k=1}^M \sum_{i=0}^k \alpha_{k,i} \frac{\partial^{k-i}}{\partial x^{k-i}} \frac{\partial^i}{\partial y^i} g(x, y), \quad (1)$$

where  $g$  is an arbitrary isotropic window function, *i.e.* a function independent of direction and approximately zero-valued outside some chosen interval. The derivatives of  $g$  with respect to  $x$  and  $y$ , which are henceforth called  $g_{k,i}$ , are called basis filters and  $\alpha_{k,i}$  are constants defining the shape of the steerable filter. For a general  $M$ th order detector  $M(M+3)/2$  basis filters are required to construct a steerable filter. Choosing the window function to be a Gaussian, *i.e.*  $g = e^{-(x^2+y^2)}$ , Jacob & Unser (2004) derived an optimal ridge detector for  $M = 2$ , using the Dirac delta function to model the ridge. The resulting steerable filter is shown in figure 1(a) and is defined by

$$h(x, y) = \sqrt{\frac{3}{4\pi}} \left( \frac{\partial^2 g}{\partial x^2} - \frac{1}{3} \frac{\partial^2 g}{\partial y^2} \right) \quad (2)$$

It can be shown that the convolution of any rotated version of the steerable filter  $h(x, y)$ , in equation (2), with the image  $f(x, y)$  can be written

$$\begin{aligned} I(\mathbf{x}, \theta) &= f(\mathbf{x}) * h(\mathbf{R}_\theta \mathbf{x}) \\ &= (\alpha_{2,0} f_{2,0} + \alpha_{2,2} f_{2,2}) \cos^2 \theta + 2(\alpha_{2,0} f_{2,1} - \alpha_{2,2} f_{2,1}) \cos \theta \sin \theta \\ &\quad + (\alpha_{2,0} f_{2,2} + \alpha_{2,2} f_{2,0}) \sin^2 \theta, \end{aligned} \quad (3)$$

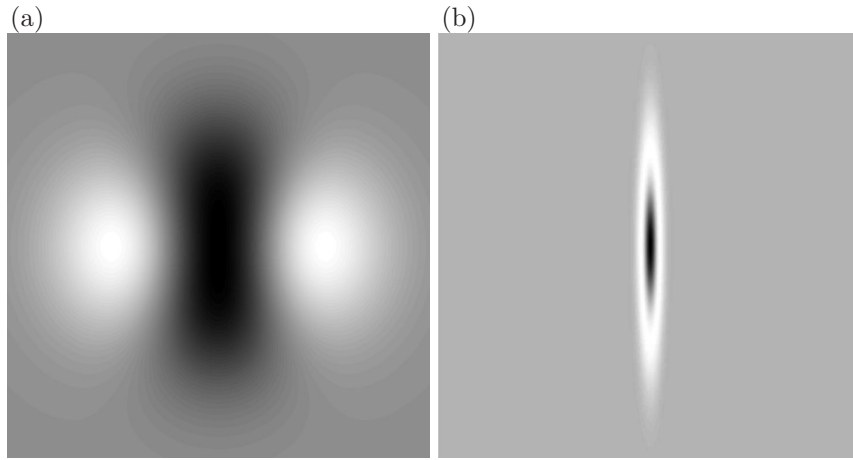


FIGURE 1. (a) The steerable ridge detector defined by equation (2) and (b) the elliptic "mexican hat" defined by equation (7) with  $b/a = 10$ .

where  $f_{k,i}$  are the convolutions of the basis filters  $g_{k,i}$  with the image  $f(x, y)$ ,  $\theta$  is the angle by which the filter is rotated and  $\mathbf{R}_\theta$  is the rotation matrix defined as

$$\mathbf{R}_\theta = \begin{pmatrix} \cos \theta & \sin \theta \\ -\sin \theta & \cos \theta \end{pmatrix}. \quad (4)$$

There are usually two solutions to the equation  $\partial I / \partial \theta = 0$ . The angle  $\theta$  that corresponds to the strongest response  $I_{max}$ , *i.e.* the highest value of  $I$ , is determined by putting both solutions into equation (3).

### 3. Measurement & analysis procedure

To evaluate if the steerable filter  $h(x, y)$ , in equation 2, is suitable for feature detection of rod-like particles, two different experiments were performed. In the first experiment, the filter was used in order to detect sharp fibres, with predefined angles, in an artificially generated image. In the other experiment fibres suspended in a viscous shear flow was studied. The data was analysed with the steerable filter, but for comparison also with another oriented filter.

#### 3.1. Artificial fibres with predefined angles

An image containing 91 artificial fibres was generated and printed on a top quality printer. The angles of the artificial fibres were well defined and one degree apart. Two different test images, shown in figure 2, were achieved by photographing the picture at two different angles. The resulting angles of the fibres, in the two different test images, are  $\theta_c = 0, 1, 2, \dots, 90$  for test image 1 and

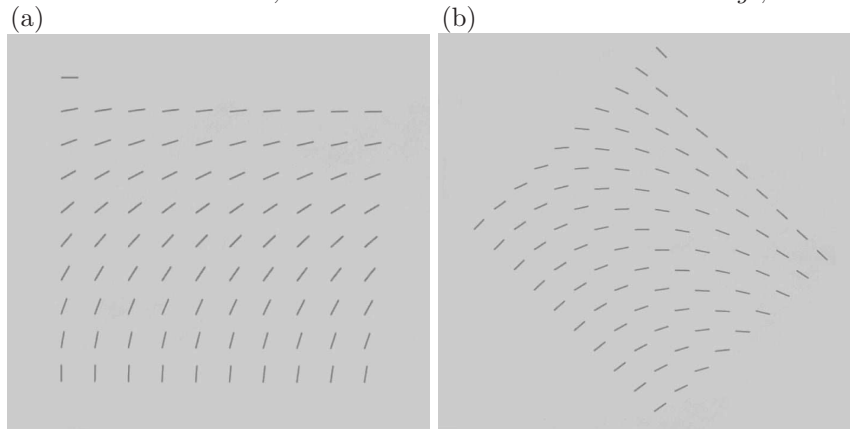


FIGURE 2. (a) Test image 1 with  $\theta_c = 0, 1, 2, \dots, 90$  (b) Test image 2 with  $\theta_c = 45, 46, 47, \dots, 135$ .

$\theta_c = 45, 46, 47, \dots, 135$  for test image 2, where  $\theta_c$  is the angle taken clockwise from the vertical direction, *i.e.*  $\theta_c = 0$  and  $90$  when a fibre is oriented in the vertical and horizontal direction, respectively.

When capturing the two test images a CCD-camera (SONY DFW-X700) was used. The camera was placed at a distance of approximately 1 m from the picture to achieve a width of the fibres close to 2 pixels. For each test image 100 images was captured and the average was calculated in order to reduce noise effects. The amplitude of each fibre was also adjusted so that all fibres had the same amplitude. This was done to reduce effects due to light variations.

The size of the steerable filter is scaled by finding the two  $x$ -positions satisfying  $h(x, y = 0) = 0$  and define two pixels, *i.e.* the width of the fibres, to be the difference of the two  $x$ -positions. Note that the steerable filter is only scaled with the width and not the length of the fibres. As a result of only scaling with the width, the convolution of the filter with the image results in high intensities at several positions along the fibres. To determine the angle of an individual fibre an averaging procedure has been imposed over all high intensity values that correspond to the fibre. Briefly a threshold value is introduced, defining how strong the convolution has to be, at a certain position, in order to belong to a fibre. Based on the orientation of the fibre at that position a searching algorithm is used to find other positions of high intensity, that belongs to the same fibre. The determined orientation  $\theta$  of the fibre is given by the average of all the angles at the positions, belonging to the fibre, where the value of the convolution exceeds the threshold.

To investigate how sensitive the method is to noise, noise has been generated and added to the two test images. If the original test image is denoted by

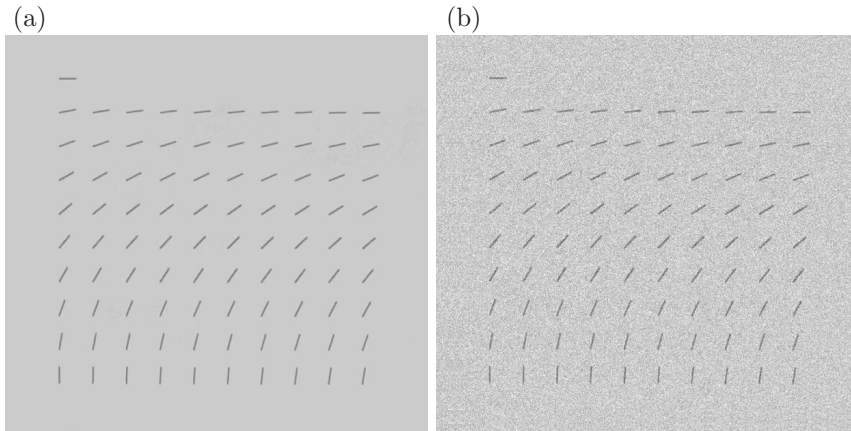


FIGURE 3. Test image 1 with different noise levels applied:  
(a)  $\sigma_s = 0$  and (b)  $\sigma_s = 1/4$ .

$f'(x, y)$  the resulting image is defined as

$$f(x, y) = f'(x, y) + n(x, y), \quad (5)$$

where  $n(x, y)$  is the noise. A random zero-mean Gaussian noise has been used to model the noise, *i.e.* the probability density function of the added noise amplitude is given by

$$n = \frac{1}{\sigma\sqrt{2\pi}} e^{(-\frac{z^2}{2\sigma^2})}. \quad (6)$$

The variable  $\sigma_s$  will be used to characterise the noise level and is defined as the standard deviation  $\sigma$  of the Gaussian noise added, normalised with the difference in amplitude between the fibres and its surroundings. A total of 500 images was generated for each noise level under study and analysed with the steerable filters algorithm. In figure 3 test image 1 is shown with added noise for two different  $\sigma_s$ .

### 3.2. Fibres suspended in a shear flow

A fibre suspension with black-dyed cellulose acetate fibres of aspect ratio  $r_p = 10$ , suspended in a viscous shear layer, has been studied experimentally, see Carlsson, Lundell & Söderberg (2006) for further details. The fibre suspension, driven by gravity, was flowing down a slightly inclined plane to generate the shear layer. To visualise the fibres a CCD-camera was mounted to capture images in a plane parallel to the solid wall plane. In the present study 100 statistically independent images is analysed, using two different feature detection algorithms. Apart from the steerable filter given by equation (2) an elliptic

”mexican hat” defined by

$$g(x, y) = \left( 4 \left[ \left( \frac{x}{a\sqrt{2}} \right)^2 + \left( \frac{y}{b\sqrt{2}} \right)^2 \right] - 2 \right) e^{-\left( \left( \frac{x}{a\sqrt{2}} \right)^2 + \left( \frac{y}{b\sqrt{2}} \right)^2 \right)} \quad (7)$$

is used, where  $a$  and  $b$  are constants defining the shape of the filter. Putting  $g = 0$  defines the ellipse  $(x/a)^2 + (y/b)^2 = 1$ . In figure 1(b) the filter is shown for  $b/a = 10$ . An elliptic mexican hat was used by Holm (2005) to determine the orientation distribution of fibres suspended in a shear flow. A difference between the mexican hat and the steerable filter is that the mexican hat is scaled both with respect to the fibre width and the fibre length. Another difference, an advantage of using the steerable filter, is that for the mexican hat a convolution has to be performed, with the image, for each angle that is to be included in the analysis. For the specific steerable filter used, only three convolutions per image are required, see equation (3).

#### 4. Results & Discussion

The steerable filter is evaluated to find the artificially generated fibres with a standard deviation of less than one degree, for moderate noise levels. Furthermore the method is compared to a robust, but more time consuming, method by analysing measurements performed on a flowing fibre suspension. Agreement is found between the two methods.

##### 4.1. Artificial fibres with predefined angles

In figure 4 the results, from analysing the the two test images, with the steerable filter, are shown. In (a) the angular deviation  $\theta_d = \theta - \theta_c$  is presented and in (b) the intensity levels from the convolutions are shown as a function of  $\theta_c$ . The solid and dashed line represents the results from analysing test image 1 and 2, respectively. There seems to be a systematical error, as a function of  $\theta$ , in the angular deviation, possibly due to the transformation to a discrete pixel form of the steerable filter. The maximum deviation is slightly above 1 degree. The intensity in figure 4(b) is normalised with the highest intensity found among the 91 fibres and it is seen that the fluctuations are moderate. It is noted though that the fluctuations are intensified for  $\theta$  close to  $\theta_c = 0 + n \cdot 45$ , where  $n$  is an integer. In these regions the maximum and minimum intensities are found, with a difference of less than 15%.

In figure 5(a) the probability density function (PDF) of  $\theta_d$ , for test images 1 and 2, is shown for various  $\sigma_s$  and in (b) the corresponding standard deviation  $\Sigma$ , skewness  $\Lambda$  and excess kurtosis  $\Gamma$  defined by

$$\Sigma = \sqrt{\frac{1}{N} \sum_{i=1}^N (\theta_d(i) - \bar{\theta}_d)^2}, \quad (8)$$

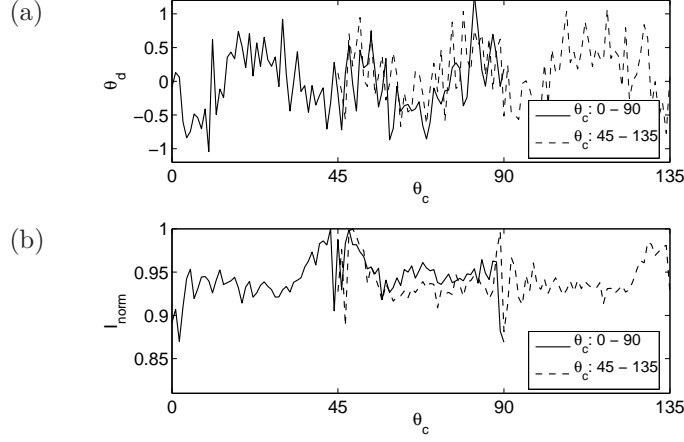


FIGURE 4. (a) The angular deviation  $\theta_d$  as a function of  $\theta_c$  for  $\sigma_s = 0$ , (b) The intensity variation with  $\theta_c$  for  $\sigma_s = 0$ . In both (a) and (b) the solid and dashed line corresponds to results from analysis of test image 1 and 2, respectively.

$$\Lambda = \frac{1}{N\Sigma^3} \sum_{i=1}^N (\theta_d(i) - \bar{\theta}_d)^3, \quad (9)$$

$$\Gamma = \frac{1}{N\Sigma^4} \sum_{i=1}^N (\theta_d(i) - \bar{\theta}_d)^4 - 3 \quad (10)$$

is shown as a function of  $\sigma_s$ . In equations (8), (9) and (10)  $\theta_d(i)$  denotes the determined angle of the  $i_{th}$  fibre and  $\bar{\theta}_d$  is the mean angular deviation. Furthermore,  $N$  is the total number of analysed fibres, *i.e.* the number of images (500 per test image) multiplied with the number of fibres per image and the number of test images. When  $\sigma_s = 0$   $\bar{\theta}_d = -0.03$  and  $0.14$  for test image 1 and 2, respectively. This may very well be an angular offset imposed when capturing the test images. It is seen, in figure 5, that the PDF of  $\theta_d$  is symmetrical around  $\theta_d = 0$ , which is also verified by  $\Lambda$  being close to zero for all  $\sigma_s$ . For small  $\sigma_s$ ,  $\Sigma$  grows slowly with  $\sigma_s$  and remains below one degree for  $\sigma_s < 1/6$ . The growth of  $\Sigma$  is however increasing with  $\sigma_s$  and is substantially larger than one degree for the higher  $\sigma_s$  under study. It is also seen that the PDF becomes flatter with an increasing  $\sigma_s$  until  $\sigma_s \approx 0.18$  where a maximum of  $\Gamma$  is found.

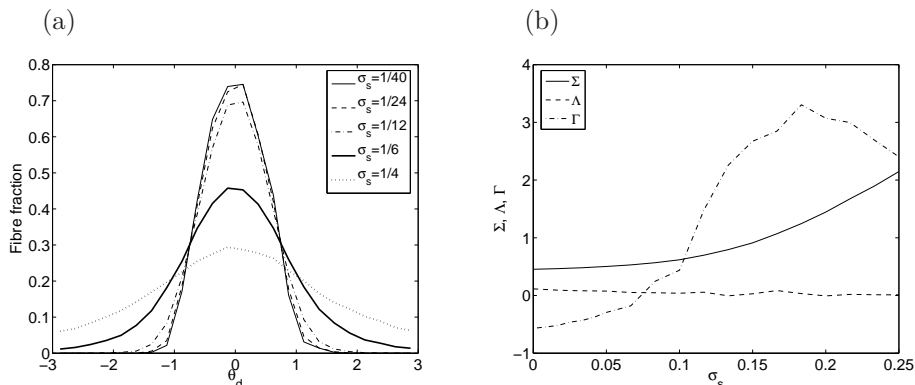


FIGURE 5. The fraction of fibres detected at different angular deviations  $\theta_d$  for various  $\sigma_s$  in (a) and  $\Sigma$ ,  $\Lambda$  and  $\Gamma$  as a function of  $\sigma_s$  in (b).

#### 4.2. Fibres suspended in a shear flow

The measurements performed on a sheared fibre suspension were analysed with both the steerable filter in equation (2) and the mexican hat in equation (7). The pixel width and length of sharp fibres, contained in the images, was approximately 2 and 20 pixels, respectively. The noise level of the captured images was  $\sigma_s \approx 0.05$ . The angular resolution of the mexican hat was chosen to be one degree, *i.e.* the filter was rotated to  $\theta = 0, 1, 2, \dots, 179$  and the convolution with the images was computed for each angle.

A total of 6903 detected fibres has been collected into bins with a range of 5 degrees and are presented as a function of the orientation  $\theta$  in figure 6. Due to symmetry around the axis of flow direction ( $\theta = 0$ ) only the orientations between  $\theta = 0$  and 90 are shown. As seen in figure 6 there is a good agreement between the two different algorithms. The detected fibres are located in a shear flow in a region from the wall to a wall normal distance of approximately two fibre lengths. However, from the figure it is not possible to determine how far from the wall the fibres are located. For a more thorough discussion of the measurements the reader is referred to Carlsson *et al.* (2006).

## 5. Conclusions

A ridge detector within the class of steerable filters has been shown to be an efficient method of locating and determining the orientation of rod-like particles, in flowing suspensions. In an image containing 91 artificially generated sharp fibres the orientation of the fibres was determined, with a standard deviation of less than one degree. A zero-mean Gaussian noise was added to the image.

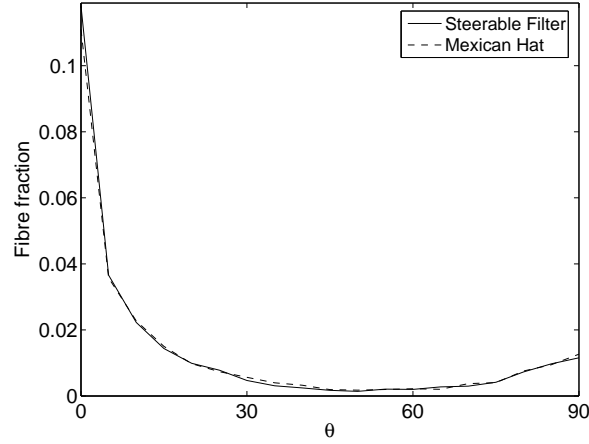


FIGURE 6. Fraction of fibres at different orientations based on analysis with a steerable filter (solid line) and with an elliptic mexican hat (dashed line).

The standard deviation remained below one degree for  $\sigma_s < 1/6$ , whereupon a more rapid increase of  $\Sigma$  was seen for larger  $\sigma_s$ .

The ridge detector was compared to an oriented elliptic mexican hat on a set of data from measurements on fibres suspended in a shear flow. Approximately the same orientation distribution was obtained with both methods. It is noted that to obtain these results the convolutions per image were 3 and 180 for the steerable filter and the mexican hat, respectively. Thus, compared to the mexican hat, the steerable filter is a very time efficient method. Another feature of the steerable filter, which could be of use, is that it only scales with the width of the fibres. The angle  $\theta$  is given for all positions along the fibres and in principal this makes it possible to determine the curvature of flexible fibres.

## References

- CARLSSON, A., LUNDELL, F. & SÖDERBERG, L. D. 2006 Fibre orientation control related to papermaking. *J. Fluids Eng.*, Accepted for publishing.
- FREEMAN, W. T. & ADELSON, E. H. 1991 The design and use of steerable filters. *IEEE T. Pattern Anal.* **13** (9), 891–906.
- HOLM, R. 2005 Fluid mechanics of fibre suspensions related to papermaking. PhD thesis, Royal Institute of Technology, Stockholm, Sweden.
- JACOB, M. & UNSER, M. 2004 Design of steerable filters for feature detection using Canny-like criteria. *IEEE T. Pattern Anal.* **26** (8), 1007–1019.